electronics

MDPI

Article

A Comparative Experimental Study of MIMO A&F and D&F Relay Nodes Using a Software-Defined Radio Platform

Randy Verdecia-Peña [1,2,*] and José I. Alonso [1,2]

[1] Information Processing and Telecommunications Center, Universidad Politécnica de Madrid, 28040 Madrid, Spain; ignacio@gmr.ssr.upm.es
[2] ETSI de Telecomunicación, Universidad Politécnica de Madrid, 28040 Madrid, Spain
* Correspondence: randy.verdecia@upm.es

Abstract: The relaying technologies in co-operative systems are considered a core element in actual and future wireless communications, assisting the network by enhancing its reliability and improving its capability through exploiting co-operativity. In this paper, a co-operative system testbed based on Software Defined Radio (SDR) through Universal Software Radio Peripherals (USRPs) and the Matlab^{TM} software is presented. The main novelty in this development of the platform is the implementation of 4G signal features, such as Physical Downlink Shared Channel (PDSCH) and Downlink Shared Channel (DL-SCH) for transport channel coding, which is one of the main contribution of the paper. The developed Multi-Input and Multi-Output (MIMO) SDR co-operative platform is capable of developing prototypes for the Relay Nodes. More specifically, the Amplify-&-Forward (A&F)—with or without Zero Forcing (ZF) and Minimum Mean Square Error (MMSE) Pre-Equalization—and Decode-&-Forward (D&F) protocols were implemented. Both Single-Input and Single-Output (SISO) and MIMO modes are supported by our testbed. The developed A&F and D&F MIMO co-operative systems in this paper utilize Orthogonal Space-Frequency Block Codes (OSFBCs) for the transmission of data symbols from the source to the destination. Our results show that relay nodes can substantially improve the Bit Error Rate (BER) and throughput in communications between the eNodeB (eNB) and User Equipment (UE). In particular, the maximum throughput achieved by conventional MIMO A&F is 9.3 Mbps at SNR = 16 dB, which is 4 Mbps higher than throughput of MIMO Non-Co-operative. It also shows the capacity improvement when considering the pre-equalization in the A&F schemes, compared to the conventional A&F Relay Node. For example, with MIMO A&F-MMSE pattern, a value of 11.8 Mbps is achieved for SNR = 16 dB, which is 84.8 % of the maximum system throughput (13.95 Mbps). On the other hand, the obtained results with D&F schemes far exceed those obtained with A&F strategies, achieving the maximum performance with the 2×2 MIMO D&F protocol from SNR = 8 dB. Furthermore, this work constitutes a first stage to the implementation of a 5G New-Radio Co-operative System platform.

Keywords: amplify-&-forward; decode-&-forward; 4G-software defined radio

check for updates

Citation: Verdecia-Peña, R.; Alonso, J.I. A Comparative Experimental Study of MIMO A&F and D&F Relay Nodes Using a Software-Defined Radio Platform. *Electronics* **2021**, *10*, 570. https://doi.org/10.3390/electronics10050570

Academic Editor: Andrey Lyakhov, Hossam S. Hassanein and Katarzyna Kosek-Szott

Received: 30 January 2021
Accepted: 25 February 2021
Published: 28 February 2021

1. Introduction

At present, mobile communications services are demanding higher data rates, more reliable transmission links, better connectivity, and satisfactory Quality of Service (QoS), as well as solutions to the challenges involved with mobility environments [1]. Several solutions have been proposed in order to improve these functionalities. Among the proposed solutions are the Co-ordinated Multi-Point transmission (CoMP) architecture, Moving Extended Cell (MEC), Carrier Aggregation (CA), and Relaying Technology [2]. The latter has been gaining momentum, as it can enable the efficient utilization of communication resources by permitting nodes to co-operate in information exchange with other, thus enhancing the QoS. In this sense, the use of Relay Nodes (RNs) presents several advantages, such as a reduction in the total transmission power, spread in the network capacity, the elimination of penetration losses in outdoor-to-indoor scenarios, and an increase in network coverage [3,4]. Accordingly, several system architectures involving Relay Nodes have been proposed in the literature [5–7], in which a stage of intermediate nodes helps the transmitter to communicate with its receiver by employing a shared radio resource [8–10]. In this context, it is not surprising that the implementation of cellular networks using RNs has become an area of significant research interest, in both industrial and academic spheres [11,12]. In addition, 3GPP has undertaken, in recent years, a major effort to study and standardize Relay Nodes, which has been collected in several releases [13–15], concluding that the technology is expected to be a key enabler for future 5G networks.

Although there is a large body of literature involving theoretical analyzes of the benefits of RNs, there are not many articles regarding the practical implementation of RNs and their viability based on empirical measurements. Currently, there exist several platforms for testbed evaluation which are suitable to examine the efficiency of Relay Nodes [16,17]. However, SDR (Software Defined Radio)-based platforms have been revealed as the most promising option for the practical implementation and evaluation of networks with relay nodes, due to their high performance and flexibility. Additionally, they provide a more suitable option for the implementation of signal processing, through the development and configuration of the Physical Layer (PHY), Medium Access Control Layer (MAC), and some Radio Link Control (RLC). The authors have developed an SDR platform using the Universal Software Radio Peripheral (USRP) and the Matlab™ software [18,19].

Different types and classifications of Relay Nodes have been proposed in the literature, as considered in the standardization by 3GPP [15]. The most straightforward way to classify RNs is by their protocol architecture. In this sense, RNs can be classified into Layer 1 (L1), Layer 2 (L2), and Layer 3 (L3). The Amplify-&-Forward (A&F) protocol fulfils of L1 RN functionalities, which simply amplifies the received signal and forwards it to the destination without performing any additional processing [20]. In this context, A&F is a simple solution and introduces almost no delay. Nevertheless, there isn't an improvement in the Signal-to-Interference-plus-Noise-Ratio (SINR) due to that the noise and interferences are also amplified. On the other hand, a Decode-&-Forward strategy symbolizes a Layer 2 Relay, in which the RF signal from the base station (eNodeB, eNB) firstly is decoded, and before of to be forwarded to the destination source it is again encoded [21]. The disadvantage main of this protocol is the delay to re-transmit the received signal, which is due to demodulation/modulation and decoding/encoding processing. However, the D&F strategy presents a high performance in comparison with the A&F scheme. Both A&F and D&F strategies are considered in this paper. It should be noted that one of the main novelties of this work is the 4G signal characteristic parameters that have been used in the implementation of the Relay Nodes. This has made it possible to perform essential signal measurements in full compliance with the 3GPP TS 38.104 standard using a high-performance spectrum analyzer.

The integration of MIMO functionalities in an RN can improve its performance and allow for more reliable transmissions [22,23]. However, MIMO A&F Relay Nodes present some problems which are yet to be solved, such as the degradation suffered by the signal between the eNB and the RN due to the propagation channel (an effect that will be transferred to the link between the Relay Node and the UE). In [24–26], various MIMO-RN schemes have been analyzed, based on knowing the Channel State Information (CSI), in order to determine the design of the optimal linear receiver. In real scenarios, the channel is unknown and, hence, needs to be estimated. Channel estimation and equalizer algorithms have been developed for MIMO-RN schemes in [27–31]. In this paper, we consider channel estimation using the pilot symbols and a Least Squares (LS) estimator. Besides, Minimum Mean Square Error (MMSE) and Zero-Forcing (ZF) pre-equalizations are adopted, prior to forwarding the signal by the MIMO A&F relay node. It should be noted that these equalization techniques have been standardized by the 3GPP for the detection of LTE signals. Furthermore, the A&F with ZF/MMSE pre-equalization have been deeply studied from a theoretical view without hardware implementation.

Motivated by the related issues, in this paper, a MIMO Relay Node Co-operative System (RNCS) through a Software Defined Radio (SDR) platform has implemented. The LTE signal which fulfils the requirement of the 3GPP has been considered. The major contribution of this paper are summarized as follows:

1. A design and implementation of a completely functional testbed framework, based on a MIMO Software Defined Radio platform and Matlab^{TM} tool have been presented, which employees the following LTE features [13]:
   - References Signals.
   - Primary Synchronization Signal (PSS).
   - Secondary Synchronization Signal (SSS).
   - Physical Broadcast Channel (PBCH).
   - Physical Format Indicator Channel (PCFIC).
   - Physical Downlink Control Channel (PDCCH).
   - Physical Downlink Shared Channel (PDSCH).

   In sense, the transmitted signal which is emulated by our eNodeB can be decoded by the MS2090A-Anritsu LTE/5G Commercial Equipment.
2. Three Amplify-&-Forward strategies have been implemented. The first A&F protocol implicates a MIMO conventional A&F scheme. Nevertheless, we focus on improving the conventional A&F relaying performance through stages of channel estimation and pre-equalization techniques. In fact, MIMO A&F protocol with Zero Forcing and Minimum Mean Square Error, have been developed, which the channel estimation has been performed by mean of Least Square (LS) estimator [32] and Bi-Cubic Interpolate (BCI) [33].
3. A MIMO Decode-&-Forward strategy has been proposed, which decoding and encoding all channel emulated by the eNodeB and considers LS channel estimator and MMSE equalization stages.
4. The implemented relaying strategies have considered stages of frequency synchronization, as well as search Cell-ID, which allows adjusting the parameters of the CP-OFDM received signal.
5. 64-QAM modulation scheme and extensive experiments have taken into account in an indoor-to-indoor environment real-world, in order to analyze the performance of the implemented protocols.

The rest of this paper is organized as follows: A brief summary of related works is given in Section 2. The system models of a two-hop MIMO, Amplify-&-Forward, and Decode-&-Forward Co-operative Communication Systems are presented in Section 3, and the mathematical models of the A&F pre-equalization schemes are described. Hardware Implementation of the RNCS through the A&F and D&F Relay Nodes is developed in Section 4. In Section 5, we present the measurement scenario. Section 6 details the experimental results and the functionality of the developed SDR platform. Finally, our conclusions are drawn in Section 7.

2. Related Works

A large amount of research evaluating the performance of co-operative wireless communications has been published, using either simulation, theory, or testbeds. In this section, we first review and evaluate some proposals, based on their obtained performance. Next, we present some co-operative test benches which have been developed and analyzed their performances. After that, we compare these results with those acquired by the platform developed and presented in this article.

Some Co-operative Communication Systems are based on the Amplify-&-Forward scheme. For example, in [34], an A&F RNCS was studied and a comprehensive set of experiments were conduced, in which it was shown that the A&F Co-operative System can provide better BER performance than a Non-Co-operative System. Similarly, in [31], an A&F protocol based on multiple antennas and a MMSE pre-equalization scheme was presented, which was compared with the ZF pre-equalization technique. In this context, the observed benefit of the pre-equalization schemes were that, at the destination, there were noticeably fewer errors when the A&F pre-equalization Co-operative System was employed. However, it was demonstrated that A&F with MMSE pre-equalization had better performance, compared with A&F with ZF pre-equalization.

On the other hand, some Co-operative Systems are based on Decode-&-Forward Relay Nodes. In [35], simulation results showed that a D&F Co-operative System can improve the average BER performance, in comparison with a Non-Co-operative system. Furthermore, in [36], the performances of the A&F and D&F have been compared, where it was observed that the Symbol Error Rate (SER) performance of the D&F was gradually enhanced, in comparison to the A&F Relay Node.

Several research works have been published which were focused on the development of test-benches for the study of co-operative communications using relay nodes in wireless networks. In [17,37], the Wireless Open-Access Research Platform (WARP) and an OFDM-MIMO A&F Relay Node were respectively presented. The WARP is a scalable and extensibly programmable wireless testbed. However, the main drawback is its limitation to a single relay, which is due to it not having an external clock interface allowing for the synchronization of multiple relays. Field Programmable Gate Arrays (FPGAs) provide another testbed platform, which has been employed in [16] to evaluate the performance of a Co-operative System. In [16], the A&F and D&F protocols were implemented, where the throughput of the proposed platforms had guaranteed high performance; nevertheless, the associated implementation and development costs hinders its usage by research communities.

On the other hand, an D&F RN has been designed, in [38], using USRP and GNU Radio, one of the most widely used SDR platforms. However, with the introduction of the Matlab$^{\text{TM}}$ software, another line to design and evaluate wireless systems has opened. In this sense, our investigation team presented, in [18], a D&F implementation using USRP and Matlab$^{\text{TM}}$, as the first step towards designing a Co-operative System with major benefit in the future. Under this background, in [19,39], the testbed was enhanced through the insertion of a new USRP with higher performance in the backhaul link (eNB-RN link), which improved the capacity of the system, given that is capable of exploiting the 2×2 MIMO scheme. In this paper, the results associated with an evaluation of our developed test bench measurement bank are presented, based on the Matlab$^{\text{TM}}$ software and USRP platform. The developed platform supports both single- and multi-relay co-operation. The results show that co-operative transmission can achieve significant performance enhancement, in terms of link reliability and end-to-end throughput.

3. System Model and Basic Assumptions

In this section, the implemented two-hop MIMO RNCS will be presented and described, which consists of a source (emulating base station, eNodeB), a Relay Node (A&F/D&F), and UE. The eNodeB is composed of two blocks, as can be seen in Figure 1: the baseband 4G signal processing block ($\mathbf{T}_{\text{BB}}$) and RF transmit chains ($\mathbf{M}_{\text{ST}}$) to up-convert the signal to a 4G frequency band, which from the point of view the implementation has been developed through the USRP, as will be presented in the following section. From Figure 1, it can be noted that a transmit diversity mode in LTE based on Alamouti codes in the frequency domain (Space-Frequency Block Coding, SFBC) has been considered. The implemented scheme exploits diversity and therefore shows the best performance when the spatial correlation between antennas is low. In our architecture, the most interesting block of the network is the Relay Node, which its function is to help the communication between the source and destination nodes. It comprises an RF receiver ($\mathbf{M}_{\text{RR}}$), implemented by USRP, a baseband signal processing algorithms associated with the implemented relaying strategies ($\mathbf{R}_{BB}$), and RF transmitter ($\mathbf{M}_{RT}$) emulated through USRP. On the other hand, the UE node consists of a RF receiver block ($\mathbf{M}_{DR}$) and the processing baseband block ($\mathbf{G}_{BB}$).

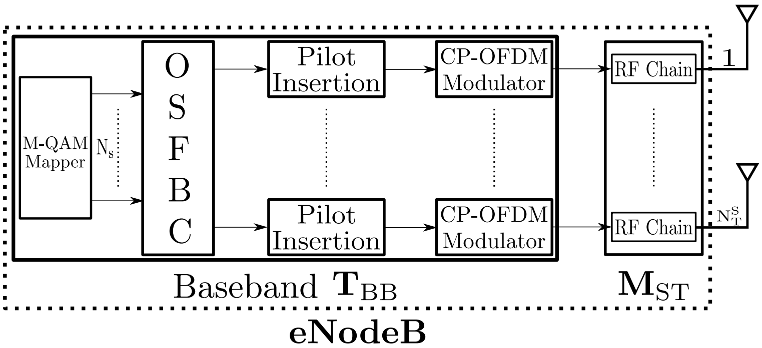

Figure 1. Baseband eNodeB architecture.

From Figure 1, we show a general MIMO eNodeB corresponding to the 3GPP LTE downlink system model [40,41]. The RNCS works in half-duplex mode and Orthogonal Space Frequency Block Code (OSFBC) matrices are used for the transmission of data symbols in the multiple antenna environment. The transmission of the OSFBC data from the eNB to the UE is performed in a two-hop manner, where we assume that at the source node, the number of transmit antennas is N_T^S and the number of data symbols is N_s. In first-hop, the source transmits $\mathbf{S} \in \mathbb{C}^{N_s \times T}$ data symbols through the baseband precoding matrix $\mathbf{T}_{BB} \in \mathbb{C}^{N_T^S \times N_s}$ and RF transmitter $\mathbf{M}_{ST} \in \mathbb{C}^{N_T^S \times N_T^S}$. Thus, the transmitted signal from the source can be expressed as

$$\mathbf{X} = \mathbf{M}_{ST}\mathbf{T}_{BB}\mathbf{S}, \tag{1}$$

where power normalization is satisfied $||\mathbf{M}_{ST}\mathbf{T}_{BB}||_F^2 = TN_T^S$. It should be noticed that the generated and configuration of the signal and channel in the eNodeB fulfil the 4G standardization of the 3GPP [13], which is one of the main novelty of our proposal. In the following subsections, we present the A&F and D&F MIMO Signal Models, techniques, and algorithms, which are included for the study of physical layer capacity.

3.1. A&F MIMO Signal Model

In this subsection, we consider the co-operative system with an A&F relaying protocol, as shown in Figure 2.

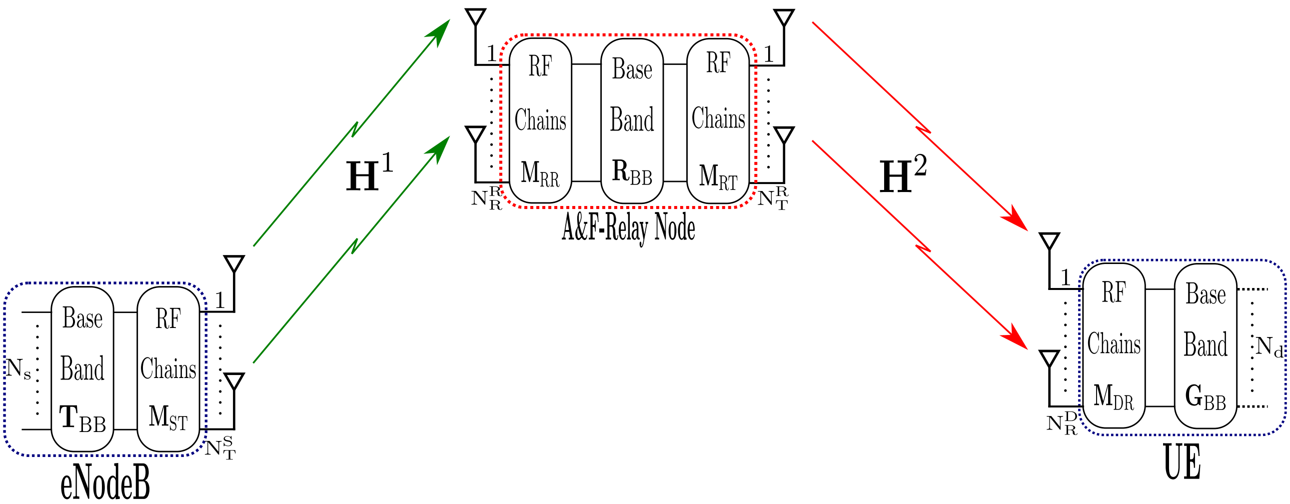

Figure 2. Two-hop A&F MIMO Relay Node Co-operative System.

Let $\mathbf{X} \in \mathbb{C}^{N_T^S \times T}$ denotes the symbols matrix to be transmitted by eNodeB. Therefore, in the first-phase, the received signal by the A&F MIMO RN can be expressed as

$$\mathbf{Y}^1_{AF} = \mathbf{H}^1\mathbf{X} + \mathbf{N}^1_{AF}, \tag{2}$$

where $\mathbf{H}^1 \in \mathbb{C}^{N_R^R \times N_T^S}$ is the channel frequency responses between the eNodeB and A&F RN, and $\mathbf{N}^1_{AF} \in \mathbb{C}^{N_R^R \times T}$ denotes noise matrix with independent and identical distributed random variables $N \sim (0, \sigma^2_{N^1_{AF}})$, where $\sigma^2_{N^1_{AF}}$ indicates the noise variance. The signal $\mathbf{Y}^1_{AF}$ is received through RF receiver chains $\mathbf{M}_{RR} \in \mathbb{C}^{N_R^R \times N_R^R}$. After that, it is precoded by matrices $\mathbf{R}_{BB} \in \mathbb{C}^{N_R^R \times N_R^R}$ and RF transmitter chains $\mathbf{M}_{RT} \in \mathbb{C}^{N_T^R \times N_R^R}$. It should be noticed that the employed strategy is the A&F, therefore, $\mathbf{R}_{BB} = \mathbf{G}_{AF}$, which depicts a diagonal matrix that on its principal diagonal contains a gain vector $\mathbf{g}_{AF}$.

Taking into account the processing above described, the transmitted signal from A&F MIMO RN is expressed by

$$\mathbf{X}_{AF} = \mathbf{M}_{RT}\mathbf{G}_{AF}\mathbf{M}^H_{RR}\mathbf{Y}^1_{AF}, \tag{3}$$

where $\mathbf{M}^H_{RR}$ denotes the hermitian matrix of $\mathbf{M}_{RR}$. In second-phase, the relay forwards the signal which is received at the destination (UE), and can be given by

$$\mathbf{Y}^2_{AF} = \mathbf{H}^2\mathbf{X}_{AF} + \mathbf{N}^2_{AF}, \tag{4}$$

where $\mathbf{H}^2 \in \mathbb{C}^{N_R^D \times N_T^R}$ denotes the channel matrix in the A&F-UE link and $\mathbf{N}^2_{AF} \in \mathbb{C}^{N_R^D \times T}$ is the components respective of Additive White Gaussian Noise (AWGN), with $N \sim (0, \sigma^2_{N^2_{AF}})$ and $\sigma^2_{N^2_{AF}}$ is the noise variance. At the UE, the received signal (4) is processed by the RF matrix $\mathbf{M}_{DR} \in \mathbb{C}^{N_R^D \times N_R^D}$ and baseband matrix $\mathbf{G}_{BB} \in \mathbb{C}^{N_d \times N_R^D}$, which are equivalent to inverse processing performed by the eNodeB. The received signal is converted to baseband frequency, and the baseband signal and physical channels are demodulated and decoded, respectively. Finally, the estimated signal of the destination can be expressed as

$$\begin{aligned}\hat{\mathbf{S}} &= \mathbf{G}^H_{BB}\mathbf{M}^H_{DR}(\mathbf{H}^2\mathbf{X}_{AF} + \mathbf{N}^2_{AF}) \\ &= \mathbf{S} + \mathbf{N}_D\end{aligned}, \tag{5}$$

where $\mathbf{G} = \mathbf{G}_{BB}\mathbf{M}_{DR}$ and $\mathbf{N}_D = \mathbf{G}^H(\mathbf{H}^2\mathbf{M}_{RT}\mathbf{G}_{AF}\mathbf{M}^H_{RR}\mathbf{N}^1_{AF} + \mathbf{N}^2_{AF})$. In the expression (5), the first and second terms represent the signal desired and noise in the Backhaul and Access Links, respectively.

3.2. A&F MIMO Signal Model with Pre-Equalization

Pre-Equalization algorithms treat all received signals as interference, except for the desired data symbols, such that the interference signals from other receiver antennas are minimized and nullified in the detection of the desired signal. In this subsection, we propose two structures for the A&F protocol based on the ZF and MMSE Pre-Equalization algorithms, considering the channel estimation of first-hop, as shown in Figure 3.

Before the Pre-Equalization step, channel estimation should be performed. In this sense, channel estimation is utilized to increase the capacity of Orthogonal Frequency Division Multiple Access (OFDMA) systems [42], improving the system performance in terms of throughput, Bit Error Rate (BER), and other parameters that are employed to measure the quality of the system. Downlink channel estimation in LTE is carried out through the use of Cell-specific Reference Signals (CRS). Pilot symbols are inserted during subcarrier mapping in both time and frequency. Furthermore, CRS are used both for demodulation and feedback calculation.

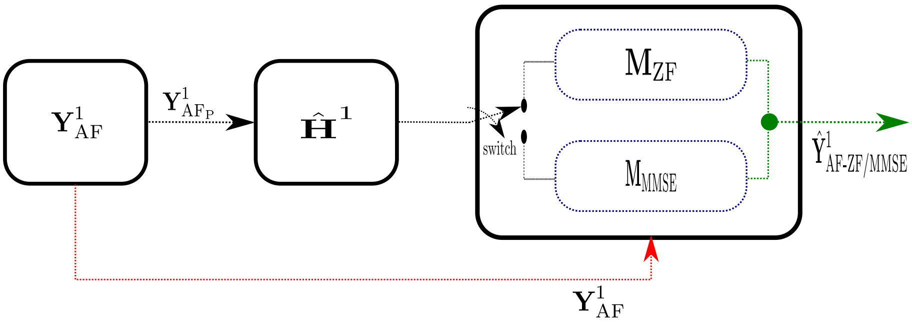

Figure 3. Pre-Equalization Schemes.

The resource blocks in LTE are allocated over M layers, K subcarriers, and L time slots. In Figure 3, the received signal described by (2) is considered. The matrix $\mathbf{Y}^1_{\text{AF}}$ is comprised of both data symbols and pilot symbols. Taking into account this assumption, $\mathbf{Y}^1_{\text{AF}}$ can be divided into two parts, the first corresponding to the pilot symbols ($\mathbf{Y}^1_{\text{AF}_\text{P}} = \mathbf{H}^1_\text{P}\mathbf{X}_\text{P} + \mathbf{N}^1_{\text{AF}_\text{P}}$) and the second to the remaining data symbols ($\mathbf{Y}^1_{\text{AF}_\text{S}}$). The Least Squares (LS) channel estimator [32] is used to equalize the channel frequency responses at pilot locations sent from different transmitter at all receiver antennas, which can be formulated as follows:

$$\hat{\mathbf{H}}^1_\text{P} = \mathbf{X}^\text{H}_\text{P}\mathbf{Y}^1_{\text{AF}_\text{P}}. \tag{6}$$

Once the frequency response of the position of the pilot symbols has been obtained, the channel response of data symbols position can be derived by interpolation employing the adjacent pilot symbols. For this, in this paper, we consider the Bi-Cubic Interpolation (BCI) method [33]. Therefore, in this second stage, $\hat{\mathbf{H}}^1$ is obtained, as performed in [39].

3.2.1. ZF Pre-Equalization Scheme

The Zero-Forcing (ZF) [43] technique is the simplest equalizer algorithm, which nullifies the interference through use of the following matrix,

$$\mathbf{M}_{\text{ZF}} = (\mathbf{H}^\text{H}\mathbf{H})^{-1}\mathbf{H}^\text{H}, \tag{7}$$

where $(\cdot)^\text{H}$ denotes the Hermitian transpose operation. Note that, the ZF pre-equalizer does not require the statistics of the noise. From Equation (2), Algorithm 1 describes the procedure of pre-equalization for SISO and MIMO techniques.

Algorithm 1: Implementation for ZF Pre-Equalizer Scheme

Input : $\mathbf{Y} = \mathbf{Y}^1_{\text{AF}}$, $\hat{\mathbf{H}} = \hat{\mathbf{H}}^1$
Output: $\hat{\mathbf{Y}}^1_{\text{AF-ZF}} = \hat{\mathbf{Y}}$
if $N^S_T == 1$ && $N^R_R == 1$ **then**
  $\hat{\mathbf{Y}} = [\hat{\mathbf{H}}^\text{H}\hat{\mathbf{H}}]^{-1}\hat{\mathbf{H}}^\text{H}\mathbf{Y}$;
else
  for $c \leftarrow 1 : N_{sub}$ **do**
    for $s \leftarrow 1 : N_{sym}$ **do**
      $\hat{\mathbf{Y}}^{(:)}_{(c,s)} = [\hat{\mathbf{H}}^{\text{H}(:,:)}_{(c,s)}\hat{\mathbf{H}}^{(:,:)}_{(c,s)}]^{-1}\hat{\mathbf{H}}^{\text{H}(:,:)}_{(c,s)}\mathbf{Y}^{(:)}_{(c,s)}$;

The received signal in the first-hop after the pre-equalization step, which is given by the output of the Algorithm 1 can be written as

$$\hat{\mathbf{Y}}^1_{\text{AF-ZF}} = \mathbf{X} + \hat{\mathbf{N}}^1_{\text{AF-ZF}}, \tag{8}$$

where $\hat{\mathbf{N}}^{1}_{\text{AF-ZF}}=(\hat{\mathbf{H}}^{1^{\text{H}}}\hat{\mathbf{H}}^{1})^{-1}\hat{\mathbf{H}}^{1^{\text{H}}}\mathbf{N}^{1}_{\text{AF}} \in \mathbb{C}^{\text{N}^{\text{R}}_{\text{R}}\times\text{T}}$ and $\hat{\mathbf{H}}^{1} \in \mathbb{C}^{\text{N}^{\text{R}}_{\text{R}}\times\text{N}^{\text{S}}_{\text{T}}}$ is the estimated channel matrix between source and A&F-ZF protocol. In A&F-ZF Relay Node, the baseband matrix $\mathbf{R}_{\text{BB}}$ is given by the product of the diagonal matrix of the A&F-ZF gain ($\mathbf{G}^{\text{ZF}}_{\text{AF}} \in \mathbb{C}^{\text{N}^{\text{R}}_{\text{T}}\times\text{N}^{\text{R}}_{\text{R}}}$) and ZF pre-equalization matrix (7) $\in \mathbb{C}^{\text{N}^{\text{R}}_{\text{R}}\times\text{N}^{\text{R}}_{\text{R}}}$. After that, the result signal is transmitted through the RF transmitter chains $\mathbf{M}_{\text{RT}} \in \mathbb{C}^{\text{N}^{\text{R}}_{\text{T}}\times\text{N}^{\text{R}}_{\text{T}}}$. Taking into account the processing in the protocol, the re-transmitted signal from the A&F-ZF Relay Node can be expressed as

$$\mathbf{X}^{\text{ZF}}_{\text{AF}} = \mathbf{M}_{\text{RT}}\mathbf{G}^{\text{ZF}}_{\text{AF}}\hat{\mathbf{Y}}^{1}_{\text{AF-ZF}}, \tag{9}$$

On the other hand, in the second-hop, the signal received by the UE can be given by

$$\mathbf{Y}^{2}_{\text{AF-ZF}} = \mathbf{H}^{2}\mathbf{X}^{\text{ZF}}_{\text{AF}} + \mathbf{N}^{2}_{\text{AF-ZF}}, \tag{10}$$

where $\mathbf{N}^{2}_{\text{AF-ZF}} \in \mathbb{C}^{\text{N}^{\text{D}}_{\text{R}}\times\text{T}}$ indicates the AWGN in the destination node, with $N \sim (0, \sigma^2_{\text{N}^2_{\text{AF}}})$ and $\sigma^2_{\text{N}^2_{\text{AF}}}$ denotes the noise variance. $\mathbf{H}^{2} \in \mathbb{C}^{\text{N}^{\text{R}}_{\text{T}}\times\text{N}^{\text{D}}_{\text{R}}}$ is the channel matrix in the access link. Finally at UE, the data symbol matrix $\mathbf{S}$ can be estimated through the following expression

$$\begin{aligned}\hat{\mathbf{S}} &= \mathbf{G}^{\text{H}}_{\text{BB}}\mathbf{M}^{\text{H}}_{\text{DR}}(\mathbf{H}^{2}\mathbf{X}^{\text{ZF}}_{\text{AF}} + \mathbf{N}^{2}_{\text{AF-ZF}}) \\ &= \mathbf{S} + \mathbf{N}_{\text{D}},\end{aligned} \tag{11}$$

where $\mathbf{G} = \mathbf{G}_{\text{BB}}\mathbf{M}_{\text{DR}}$ and $\mathbf{N}_{\text{D}} = \mathbf{G}^{\text{H}}(\mathbf{H}^{2}\mathbf{M}_{\text{RT}}\mathbf{G}^{\text{ZF}}_{\text{AF}}\hat{\mathbf{N}}^{1}_{\text{AF-ZF}} + \mathbf{N}^{2}_{\text{AF-ZF}})$ is the received signal not desired.

3.2.2. MMSE Pre-Equalization Scheme

In order to maximize the equalization Signal-to-Noise Ratio (SNR), the MMSE [43] pre-equalizer can be used, which is given as

$$\mathbf{M}_{\text{MMSE}} = (\mathbf{H}^{\text{H}}\mathbf{H} + \sigma^2_n\mathbf{I})^{-1}\mathbf{H}^{\text{H}}, \tag{12}$$

where $\mathbf{H}^{\text{H}}$ describes the hermitian transpose matrix of the channel and σ^2_n is the statistical information of the noise. The baseband processing by the A&F-MMSE protocol is given by Algorithm 2, which taking into account the received signal (2) and MMSE matrix (12), this algorithm performs the pre-equalization for SISO and MIMO strategies.

Algorithm 2: Implementation for MMSE Pre-Equalizer Scheme

```
Input  : Y = Y^1_AF, Ĥ = Ĥ^1, N̂_0
Output: Ŷ^1_AF-MMSE = Ŷ
if N^S_T == 1 && N^R_R == 1 then
    Ŷ = (Ĥ^H Ĥ + N̂_0)^{-1} Ĥ^H Y;
else
    for c ← 1 : N_sub do
        for s ← 1 : N_sym do
            Ŷ^(:)_(c,s) = ((Ĥ^{H(:,:)}_(c,s) Ĥ^{(:,:)}_(c,s) + N̂_0 I)^{-1} / I) Ĥ^{H(:,:)}_(c,s) Y^(:)_(c,s);
```

Considering the Algorithm 2 output, the pre-equalized signal is given by

$$\hat{\mathbf{Y}}^{1}_{\text{AF-MMSE}} = \mathbf{X} + \hat{\mathbf{N}}^{1}_{\text{AF-MMSE}}, \tag{13}$$

where $\hat{\mathbf{N}}^1_{\text{AF-MMSE}} = (\hat{\mathbf{H}}^{1^{\text{H}}}\hat{\mathbf{H}}^1 + \sigma^2_{\text{N}^1_{\text{AF}}}\mathbf{I})^{-1}\hat{\mathbf{H}}^{1^{\text{H}}}\mathbf{N}^1_{\text{AF}} \in \mathbb{C}^{\text{N}^{\text{R}}_{\text{R}}\times\text{T}}$ and $\hat{\mathbf{H}}^1 \in \mathbb{C}^{\text{N}^{\text{R}}_{\text{R}}\times\text{N}^{\text{S}}_{\text{T}}}$ is the estimated channel frequency responses between eNodeB and A&F-MMSE strategy. Therefore, the re-transmitted signal from the A&F-MMSE protocol can be written as

$$\mathbf{X}^{\text{MMSE}}_{\text{AF}} = \mathbf{M}_{\text{RT}}\mathbf{G}^{\text{MMSE}}_{\text{AF}}\hat{\mathbf{Y}}^1_{\text{AF-MMSE}}, \tag{14}$$

where $\mathbf{G}^{\text{MMSE}}_{\text{AF}} \in \mathbb{C}^{\text{N}^{\text{R}}_{\text{T}}\times\text{N}^{\text{R}}_{\text{R}}}$ denotes the diagonal matrix of the A&F-MMSE gain, $\hat{\mathbf{Y}}^1_{\text{AF-MMSE}} \in \mathbb{C}^{\text{N}^{\text{R}}_{\text{R}}\times\text{T}}$, and RF transmitter chains $\mathbf{M}_{\text{RT}} \in \mathbb{C}^{\text{N}^{\text{R}}_{\text{T}}\times\text{N}^{\text{R}}_{\text{T}}}$. On the other hand, the received signal in the UE after re-transmission at the Relay Node can be expressed as

$$\mathbf{Y}^2_{\text{AF-MMSE}} = \mathbf{H}^2\mathbf{X}^{\text{MMSE}}_{\text{AF}} + \mathbf{N}^2_{\text{AF-MMSE}} \tag{15}$$

where $\mathbf{N}^2_{\text{AF-MMSE}} \in \mathbb{C}^{\text{N}^{\text{D}}_{\text{R}}\times\text{T}}$ denotes the AWGN at the UE, $N \sim (0, \sigma^2_{\text{N}^2_{\text{AF}}})$ and $\sigma^2_{\text{N}^2_{\text{AF}}}$ represents the noise variance. $\mathbf{H}^2 \in \mathbb{C}^{\text{N}^{\text{R}}_{\text{T}}\times\text{N}^{\text{D}}_{\text{R}}}$ is the channel matrix in the access link. Considering the data processing of the UE through the baseband $\mathbf{G}_{\text{BB}}$ and RF receiver chains $\mathbf{M}_{\text{DR}}$, the estimated received data at the destination can be obtained by

$$\begin{aligned}\hat{\mathbf{S}} &= \mathbf{G}^{\text{H}}_{\text{BB}}\mathbf{M}^{\text{H}}_{\text{DR}}(\mathbf{H}^2\mathbf{X}^{\text{MMSE}}_{\text{AF}} + \mathbf{N}^2_{\text{AF-MMSE}}) \\ &= \mathbf{S} + \mathbf{N}_{\text{D}}\end{aligned}, \tag{16}$$

where $\mathbf{G} = \mathbf{G}_{\text{BB}}\mathbf{M}_{\text{DR}}$ and $\mathbf{N}_{\text{D}} = \mathbf{G}^{\text{H}}(\mathbf{H}^2\mathbf{M}_{\text{RT}}\mathbf{G}^{\text{MMSE}}_{\text{AF}}\hat{\mathbf{N}}^1_{\text{AF-MMSE}} + \mathbf{N}^2_{\text{AF-MMSE}})$.

3.3. D&F MIMO Signal Model

In this subsection, the D&F Co-operative System will be addressed. In the first-hop, the signal is received by the D&F Relay Node which, before re-transmitting (second-hop), decodes the transmitted symbols from eNB, encodes these symbols into an OSFBC (having the same structure as used by eNB) and, then, transmits it over the access link (i.e., the D&F–UE link), as shown in Figure 4.

Let $\mathbf{X} \in \mathbb{C}^{\text{N}^{\text{S}}_{\text{T}}\times\text{T}}$ denotes the symbols matrix by the eNB in the first-hop of data transmission, where T is the number of used subcarriers for the transmission and $\text{N}^{\text{S}}_{\text{T}}$ is the number of transmit antennas. Therefore, the received data at the D&F relay node in a block can be expressed as

$$\mathbf{Y}^1_{\text{DF}} = \mathbf{H}^1\mathbf{X} + \mathbf{N}^1_{\text{DF}}, \tag{17}$$

where $\mathbf{H}^1 \in \mathbb{C}^{\text{N}^{\text{R}}_{\text{R}}\times\text{N}^{\text{S}}_{\text{T}}}$ represents the channel frequency responses of the eNB-D&F link. On the other hand, $\mathbf{N}^1_{\text{DF}} \in \mathbb{C}^{\text{N}^{\text{R}}_{\text{R}}\times\text{T}}$ represents the Additive White Gaussian Noise (AWGN) matrix of the Backhaul Link (i.e., the eNB–D&F link). Furthermore, the elements of the noise matrix are complex Gaussian random variables with $N \sim (0, \sigma^2_{\text{N}^1_{\text{DF}}})$ and $\sigma^2_{\text{N}^1_{\text{DF}}}$ is the noise variance. In the D&F Relay Node, the decoding and encoding of the received signal (17) is carried out by two stages, as can be seen in Figure 4. Firstly, the decoding processing is performed through the receive baseband matrix $\mathbf{R}_{\text{BBR}} \in \mathbb{C}^{\text{N}_{\text{s}}\times\text{N}^{\text{R}}_{\text{R}}}$ and RF receiver chains matrix $\mathbf{M}_{\text{RR}} \in \mathbb{C}^{\text{N}^{\text{R}}_{\text{R}}\times\text{N}^{\text{R}}_{\text{R}}}$. Therefore, as result of the first stage, an estimated data symbols matrix $\tilde{\mathbf{S}} \in \mathbb{C}^{\text{N}_{\text{s}}\times\text{T}}$ is obtained. Thus, the encoding processing is carried out by the transmit baseband matrix $\mathbf{R}_{\text{BBT}} \in \mathbb{C}^{\text{N}^{\text{R}}_{\text{T}}\times\text{N}_{\text{s}}}$ and RF transmit chains matrix $\mathbf{M}_{\text{RT}} \in \mathbb{C}^{\text{N}^{\text{R}}_{\text{T}}\times\text{N}^{\text{R}}_{\text{T}}}$, consequently, the transmitted signal by the Relay Node is given by

$$\hat{\mathbf{X}} = \mathbf{M}_{\text{RT}}\mathbf{G}_{\text{DF}}\mathbf{R}_{\text{BBT}}\tilde{\mathbf{S}}, \tag{18}$$

where $\mathbf{G}_{\text{DF}} \in \mathbb{C}^{\text{N}^{\text{R}}_{\text{T}}\times\text{N}^{\text{R}}_{\text{T}}}$ represents a diagonal matrix with principal diagonal containing a gain vector ($\mathbf{g}_{\text{DF}}$). On the other hand, the received signal at the UE after performing demodulation, modulation, and re-transmission at the relay node can be expressed by

$$\mathbf{Y}^2_{\text{DF}} = \mathbf{H}^2\hat{\mathbf{X}} + \mathbf{N}^2_{\text{DF}}, \tag{19}$$

where $\hat{\mathbf{X}}$ is the $\mathrm{N_T^R} \times \mathrm{T}$ matrix forwarded by the relay node after the decoding of $\mathbf{X}$, $\mathbf{H}^2 = [h^1_{i,j}] \in \mathbb{C}^{\mathrm{N_R^D} \times \mathrm{N_T^R}}$ is the channel matrix of the access link, $\mathbf{N}^2_{\mathrm{DF}} \in \mathbb{C}^{\mathrm{N_R^D} \times \mathrm{T}}$ contains the AWGN with $N \sim (0, \sigma^2_{\mathrm{N}^2_{\mathrm{DF}}})$, and $\sigma^2_{\mathrm{N}^2_{\mathrm{DF}}}$ indicates the noise variance. At the UE, baseband matrix $\mathbf{G}_{\mathrm{BB}} \in \mathbb{C}^{\mathrm{N_d} \times \mathrm{N_R^D}}$ and RF receive chains matrix $\mathbf{M}_{\mathrm{DR}} \in \mathbb{C}^{\mathrm{N_R^D} \times \mathrm{N_R^D}}$ are used to obtain the desired symbols and can be expressed as

$$\begin{aligned} \hat{\mathbf{S}} &= \mathbf{G}^{\mathrm{H}}_{\mathrm{BB}} \mathbf{M}^{\mathrm{H}}_{\mathrm{DR}} (\mathbf{H}^2 \hat{\mathbf{X}} + \mathbf{N}^2_{\mathrm{DF}}) \\ &= \tilde{\mathbf{S}} + \mathbf{N}_{\mathrm{D}} \end{aligned}, \tag{20}$$

where $\mathbf{N}_{\mathrm{D}} = \mathbf{G}^{\mathrm{H}} \mathbf{N}^2_{\mathrm{DF}}$ and $\mathbf{G} = \mathbf{G}_{\mathrm{BB}} \mathbf{M}_{\mathrm{DR}}$. In (20), the first term is the desired signal and the second term is the noise, which represents the noise in access link at the Decode-&-Forward (D&F) RNCS, respectively.

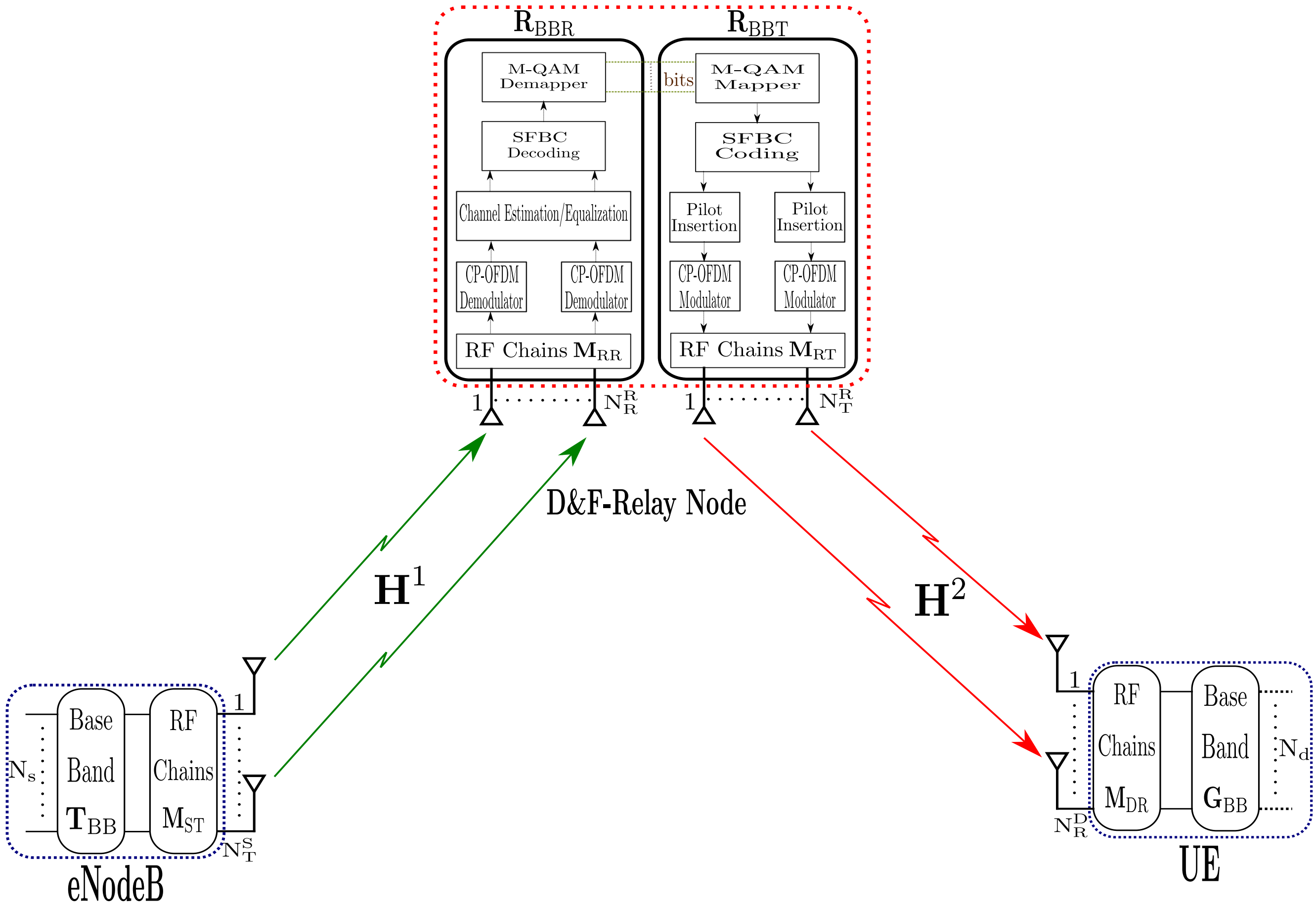

Figure 4. Two-hop D&F MIMO Relay Node Co-operative System.

4. Hardware Implementation of the RNCS

In this section, a Relay Node Co-operative System employing SDR platform is presented. A&F and D&F Relay Nodes were implemented, where Frequency Division Duplexing (FDD-LTE), multiple antennas (2 × 2 MIMO), and in-band operation—that is, the two links (backhaul and access links) have the same frequencies—are considered. The goal of this paper is to examine the downlink performance of the UE in a real scenario using these architectures.

4.1. Co-Operative System Implementation

In this subsection, we describe the developed MIMO SDR platform for testing and characterizing the A&F and D&F Relay Nodes. For their implementation, the NI-USRP

2944R and NI-USRP 2901R were used. Their operating frequencies range from 70 MHz to 6 GHz, which is considered as sufficient to take on the flexibility demands of our platform. Each board can hold two RF chains (2Tx/2Rx). Furthermore, they can support a sample rate up to 56 MHz, which is sufficient to record an LTE signal (with maximum bandwidth of 20 MHz). These technical parameters make them suitable for the required functionalities.

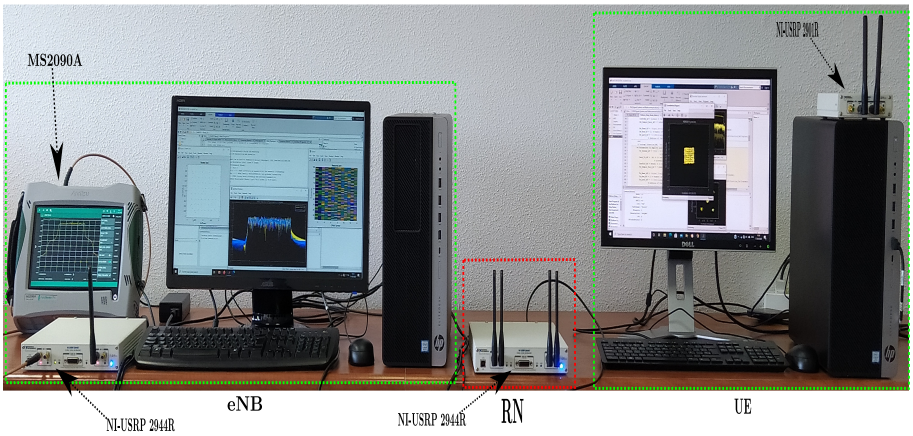

Figure 5. Testbed Environment for A&F and D&F Relay Nodes system.

The developed testbed system is shown in Figure 5. It is composed of one evolved Node-B (eNB), which is achieved with one NI-USRP 2944R board and the Matlab^{TM} software. Connection from a PC to the NI-USRP 2944R is performed through the NI-IMAQdx GigE Vision High-Performance Driver, a 10 Gigabit Ethernet Card for Desktop, and a 10 Gigabit ethernet cable. Figure 6 shows the occupied bandwidth (4.57 MHz) of the transmitted signal by emulated eNB, which was measured at the output of the NI-USRP 2944R through the MS2090A Field Master Pro of Anritsu. The transmitted frequency error was approximately 344 Hz, which could be perfectly corrected with the implemented frequency offset correction algorithms. The total channel power transmitted by the emulated eNB was approximately 16 dBm, which fulfils the requirement demanded by the 3GPP in [44] for the downlink at 5 MHz channel bandwidth.

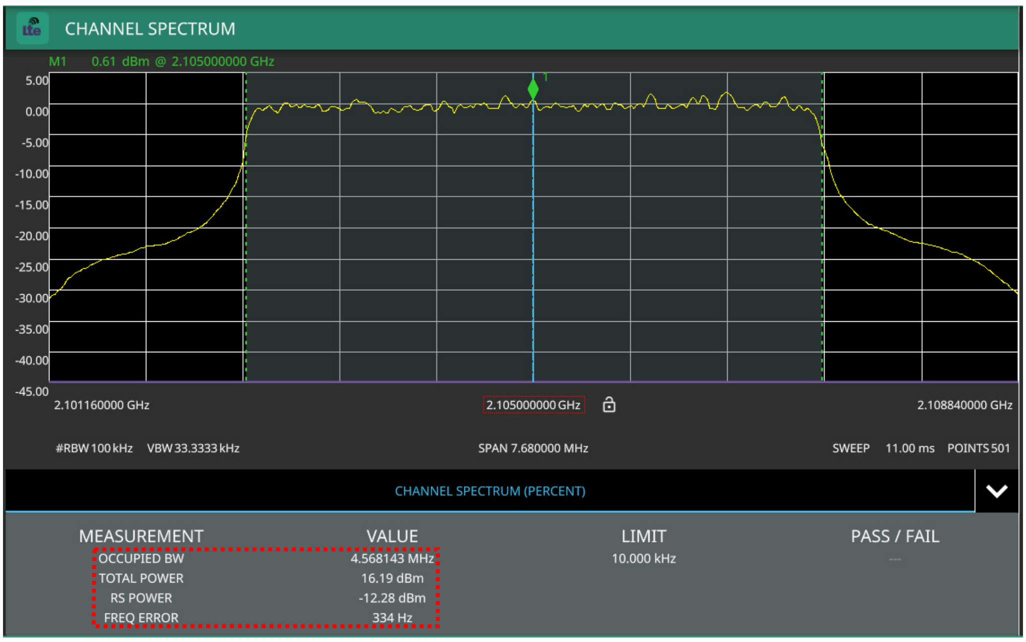

Figure 6. Bandwidth occupied by the signal transmitted by the emulated eNB.

The demodulation of the transmitted signal by means of the MS2090A equipment is presented in Figure 7. The obtained information from Figure 7 shows the Error Vector Magnitude (EVM) of the PBCH and PDSCH. Furthermore, the power of the several reference signals and of the PBCH can be observed, which were adjusted to the 3GPP standard in [44].

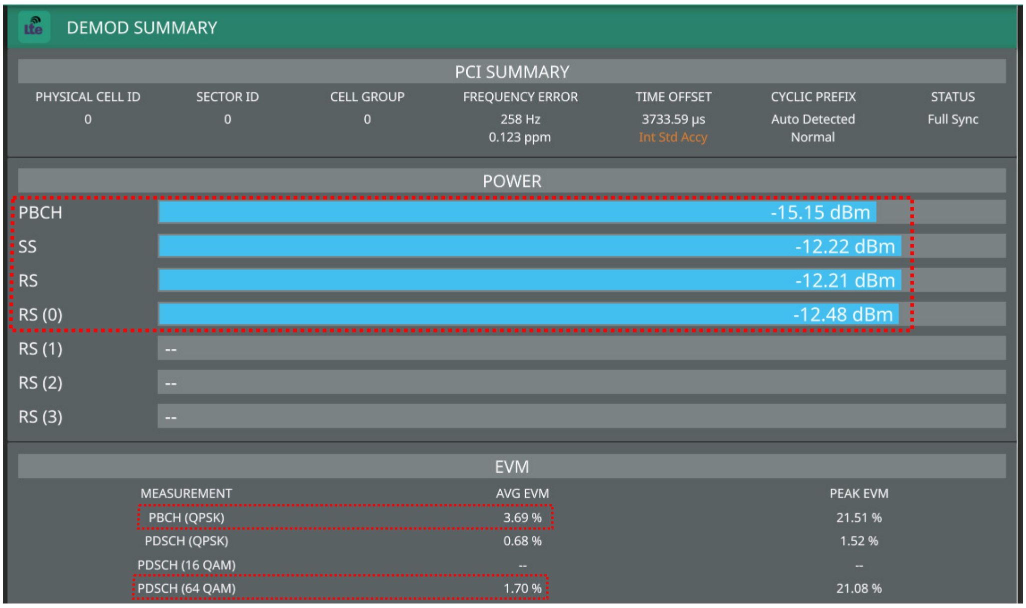

Figure 7. Transmitted Signal Demodulation from eNB.

On the other hand, the A&F and D&F Relay Nodes were implemented using a PC, the Matlab^{TM} software, and an NI-USRP 2944R. The NI-IMAQdx GigE Vision High-Performance Driver, 10 Gigabit Ethernet Card for Desktop, and 10 Gigabit ethernet cable were also used for the connection. The User Equipment (UE) was developed by employing a PC, the Matlab^{TM} software, and an NI-USRP 2901R, where the connection from the PC to the USRP was performed through USB 3.0. The antennas used for the experiments were general-purpose LTE and Wi-Fi antennas which work on the 700–960 MHz and 1710–2700 MHz bands, respectively. They had a gain of 5 dBi and an impedance of 50 Ω. They had SMA connectors, which were compatible with the USRP connectors. Furthermore, the implemented Relay Nodes are an in-band RNs, that is, the reception and transmission frequencies are the same, but the transition from one to the other is done in different time intervals. On the other hand, the problem of coupling and interferences between the antennas has been studied experimentally. In this sense, several measurements have been made at different positions of the receiving and transmitting antennas of the eNB, RNs, and UE to determine their optimal position and minimize interference.

4.2. A&F Relay Node Implementation

In this subsection, we propose our scheme to implement MIMO A&F Relay Nodes with standardized LTE signal by 3GPP. Here, we present A&F protocol without and with pre-equalization techniques. Therefore, the implemented A&F Relay Node estimates the channel or not, depending on whether this functionality is activated, as shown in Figure 8. In the first phase, the IQ is captured with the MIMO NI-USRP 2944R platform. After acquiring the received information, the signal is saved in the buffer (processing signal block) and, considering the selected functionality, switch 1 will select position 1 (Amplify-&-forward) or 2 (pre-equalization and Amplify-&-forward). If position 2 is selected, before pre-equalization, it must perform a cell search and another step. This involves acquiring slot and frame synchronization, looking up the cell identity, and decoding the Master Information Block (MIB). In the basic structure, a configuration structure taking into account the sample rate of the MIMO NI-USRP 2944R platform is performed, in which a duplex mode (FDD), cyclic prefix (Normal), and number of resource blocks (depending on the sample rate of the SDR) are assumed.

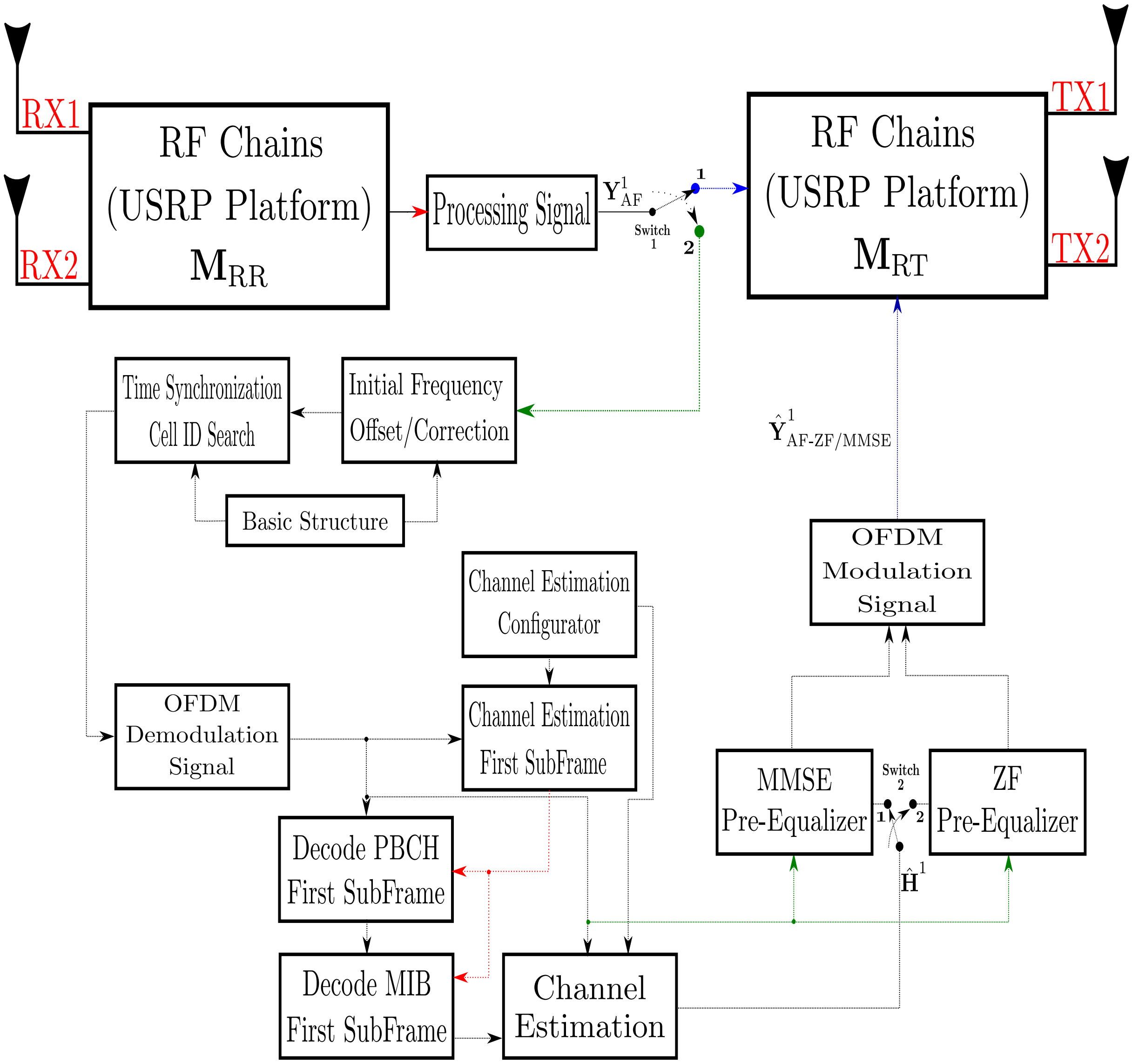

Figure 8. MIMO Amplify-&-Forward Relay Node Processing Blocks.

Prior to searching the Cell ID, any significant frequency offset must be estimated and removed, without which many errors would propagate. Furthermore, the Primary Synchronization Signal (PSS) and Secondary Synchronization Signal (SSS) are produced. The PSS and SSS are detected by employing the time- and frequency-domain correlation. Therefore, the timing offset and cell identity are obtained. Then, in order to establish the quality of the correlation, the correlation for each of the three possible primary cell identities is computed.

After the steps described above, the MIMO-OFDM signal is demodulated. The first task after MIMO-OFDM demodulation is to perform channel estimation of the first subframe, which is carried out by making use of the configurate channel estimation block. Subsequently, the PBCH is demodulated; the main goal of this channel is to hold up the MIB that specifies the parameters, in order to determine the Full Bandwidth. All parameters are known when the decode MIB block is performed. Now, the relay node is ready to perform channel estimation of the complete signal bandwidth, which is carried out by the channel estimation block. The output of the channel estimation and MIMO-OFDM demodulation are passed through the MMSE and ZF equalizers, for which the equalization type is selected using switch 2. Finally, the equalized signal is modulated(MIMO-OFDM) and transmitted through an the RF transmit chains of the MIMO NI-USRP 2944R.

4.3. D&F Relay Node Implementation

In this subsection, a MIMO Decode-&-Forward Relay Node using the developed SDR Platform is implemented. A simplified flowchart of the MIMO Decode-&-Forward Relay Node can be seen in Figure 9.

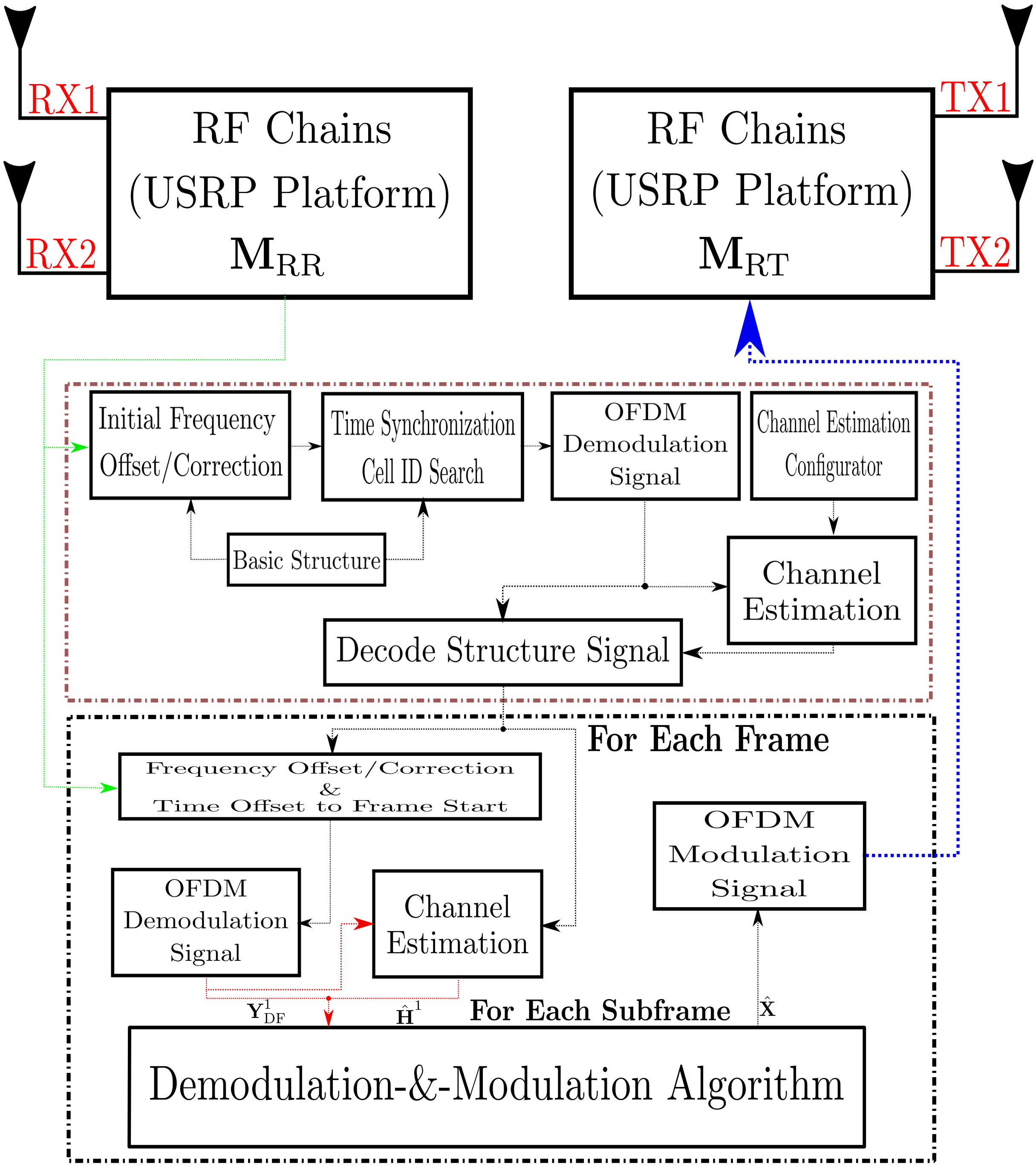

Figure 9. MIMO Decode-&-Forward Relay Node Processing Blocks.

First, the IQ signals are captured by the RF receive chains of the MIMO NI-USRP 2944R platform. After acquisition of the data symbols, any significant frequency deviation must be estimated and eliminated, without which many errors would propagate. Furthermore, the Primary Synchronization Signal (PSS) and Secondary Synchronization Signal (SSS) are produced. The PSS and SSS are detected by employing the time- and frequency-domain correlation. Therefore, the time offset synchronization and cell identity in the Time Synchronization & Cell ID Search block are obtained. Then, in order to establish the quality of the correlation, the correlation for each of the three possible primary cell identities is computed. The Basic Structure block is a configuration structure, taking into account the sample rate of the SDR. Duplex mode (FDD), Cyclic Prefix, and a number of resource blocks (depending on the sample rate of the SDR) are assumed.

After the steps described above, the MIMO-OFDM signal is demodulated. The first task after MIMO-OFDM demodulation is to perform channel estimation of the first subframe, which is carried out by making use of the Channel Estimation Configurator block. The Channel Estimation block is performed in two steps: First, the frequency responses for the subcarriers of the pilot symbols are determined, based on the Least Squares (LS) estimator. On the other hand, from the first step, the frequency responses of the subcarriers of the data symbols can be derived by interpolation methods employing the adjacent pilot symbols. For this, we use the 2D Bi-Cubic (BC) interpolation method [33]. The outputs of the OFDM Demodulation Signal and Channel Estimation blocks are used as the input of the Decode Structure Signal, which determines the parameters to obtain the full bandwidth. Nevertheless, now that the signal parameters are known, the received signal is resampled to the nominal sampling rate. Afterwards, the Relay Node can carry out the full received signal demodulation and, so, perform the channel estimation. Finally, the demodulated MIMO received signal ($\mathbf{Y}^1_{\mathrm{DF}}$) and the estimated channel matrix ($\hat{\mathbf{H}}^1$) are processed through the Demodulation-&-Modulation Algorithm Processing Blocks in Figure 10, which is performed to each subframe.

This Processing Block in Figure 10 executes the demodulation and modulation of physical, control, and data channels, as well as determining other reference signals. In the 4G communication networks, the PDCCH used to provide physical layer signaling to support MAC layer operation. Each PDCCH carries the message known as the Downlink Control Information (DCI) for the UE. DCI contains the information about resource scheduling for downlink and uplink, transmit power commands (TPC), etc. On the other hand, PBCH is a control channel (can be found in subframe 0 of each radio frame), which has the aim of transporting basic information about the net, named by Master Information Block (MIB). This information contains: four bits to identify the canalization used in the cell, three bits to define the channel PHICH(Physical Hybrid ARQ Indicator Channel) structure that is used to transport recognition information about the HARQ (Hybrid Automatic Repeat Request) mechanism and seven bits in order to identify the frame number (System Frame Number, SFN). On the other hand, the data symbols are carried out by the PDSCH, particularly, SIBs (System Information Blocks) are transported by this physical channel. Several modulation options can be applied to this channel, including Q-PSK, 16-QAM, and 64-QAM, which the 64-QAM scheme has been employed in our platform, as well as is flexible and can be considered Q-PSK and 16-QAM. PDSCH is used to transmit the Downlink Shared Channel, which acts as the transport channel used for transmitting downlink data (a transport block). The resultant signal at the output of scheme in Figure 10, is modulated through the OFDM Modulation RF transmit chains in the MIMO NI-USRP 2944R platform.

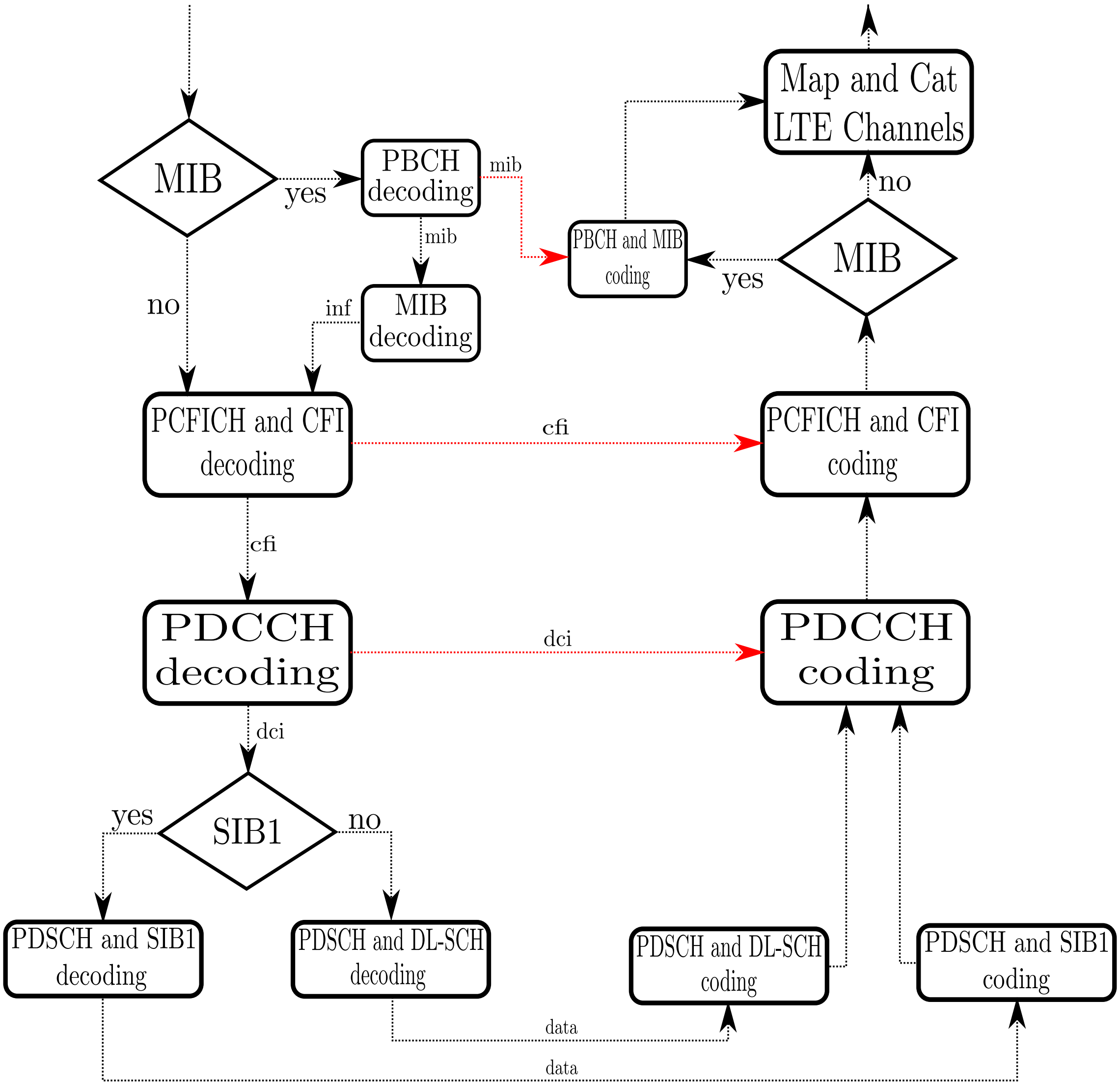

Figure 10. Demodulation-&-Modulation Algorithm Processing Blocks.

5. Measurement Scenario

In this section, the measurement scenario to the study of MIMO A&F and D&F relay Node through the implemented platform is presented. A series of measurements in an indoor scenario—in particular, on the fourth floor of building C of the School of Telecommunications at the Polytechnic University of Madrid—were carried out, in order to verify the operations of the relay nodes with the developed testbed.

The LTE network real-scenario in Figure 11 is composed of one eNodeB, which will serve the one UE through the RN (A&F, A&F-ZF, A&F-MMSE or D&F). Besides, we considered the scenario shown in Figure 11, where the eNB and RN have Line-of-Sight (LOS) with distance between them of 16 meters. On the other hand, the UE was placed inside the room C-404, positioned about 22 and 9 meters, respectively, from the eNB and the RN. Furthermore, inside the office, tables, chairs, and informatics equipment were present. It should be noticed that the UE node has Non-Line-of-Sight (NLOS) with respect to the eNodeB and the RN, and due to that an experimental measurement scenario is taken into account, the path-loss, and fading effects are considered.

Our results characterize the performance of the downlink, obtained by means of an eNB which was emulated using an LTE signal generated using the Matlab LTE ToolBox. Furthermore, the simulation parameters that were used during the realization of the system were as given in Table 1. For each transmission (20), 50 Frames were sent, where the relay processed the signal and forward it, and the UE carried out two kinds of decoding: Decoding from the eNB (direct link) and from the RN (access link). The UE calculated the considered metrics for the two kinds of link-level individually.

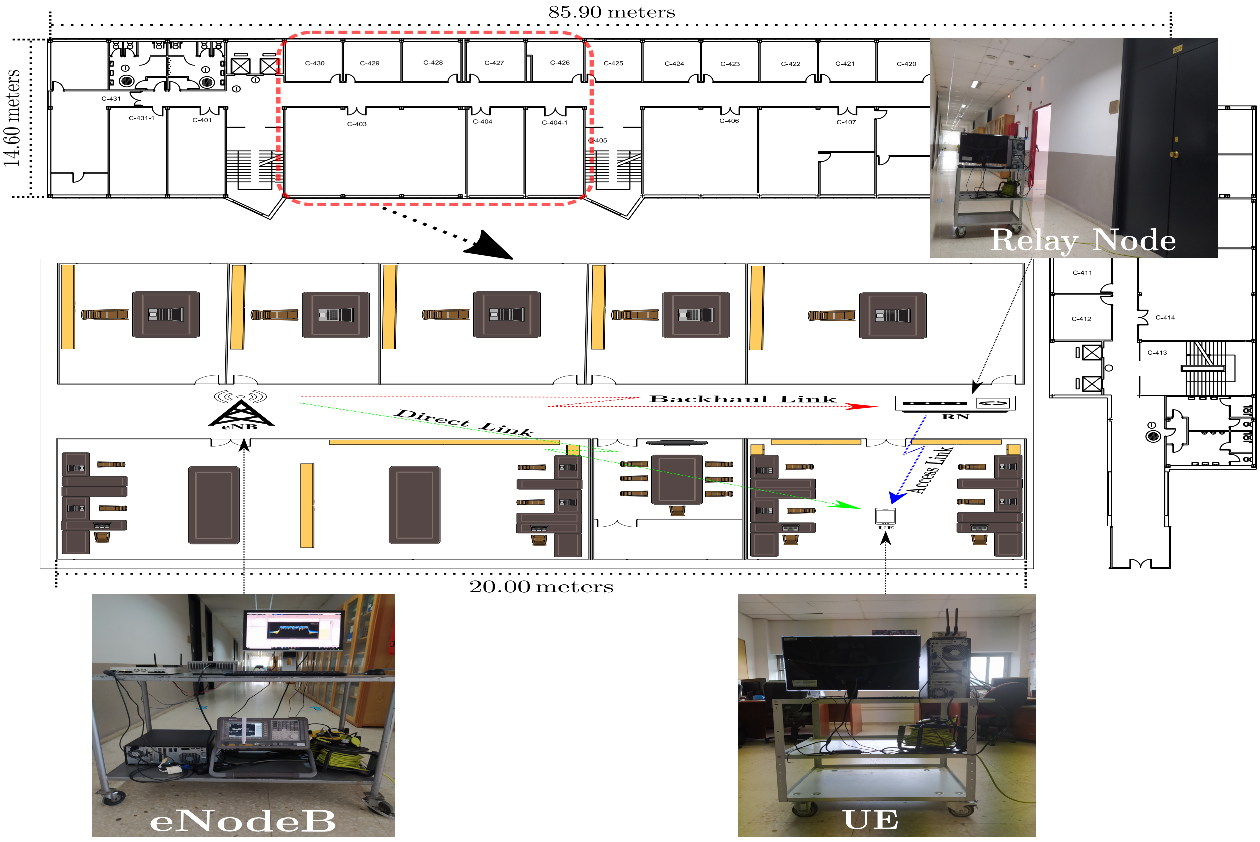

Figure 11. Indoor-to-Indoor experimental scenario with MIMO Relay Node.

Table 1. Main parameters to emulate the eNB.

Parameters	Values
Signal bandwidth, F_s	5 MHz
Carrier Frequency, f_s	2.105 GHz
Tx/Rx schemes	SISO and 2 × 2 MIMO
LTE Duplex Scheme	LTE-FDD
RMC number	R.6 and R.11
Modulation	64-QAM
Target Code Rate	3/4
Samples Rate	7.68 MHz
Cyclic Prefix	Normal
Number of FFT	512
Number of Subcarriers × Symbols in a Frame	300 × 140
Number of pilot symbols per Frame	8000
Number of data symbols per Frame	34,000
Subcarrier spacing	15 kHz
Number of Cell ID	0
Number of transmission	20

On the other hand, the authors have performed several measurements to experimentally estimate the SNR using the MS2090A handheld Spectrum Analyzer. In the NI-USRP 2944R used to emulate the eNB, its internal gain has been varied and the SNR on the receiver side has been estimated with the MS2090A, for each transmitted power level. This measurement has been carried out for different levels of gain transmitted by the NI-USRP 2944R, using the average of each point as the SNR value.

6. Experimental Results and Discussion

Our experiments were based on the MIMO RNCS introduced in Section 4. Section 6.1 compares the effect introduced by the Pre-Equalization stage in the A&F Relay Node, while Section 6.2 provides a range of simulation results to evaluate the physical layer BER performance and MAC layer throughput on the hardware implementation of the RNCS described above.

6.1. Impact of Pre-Equalization Stage in A&F RN

The impact introduced by the Pre-Equalization stage in the A&F Relay Node was investigated using the Error Vector Magnitude (EVM) metric.

Figure 12 shows the obtained results for the Cumulative Distribution Function (CDF) of the re-transmitted Resource Grid (RG) of the A&F schemes, with respect to the RMS EVM [%]. The red plot represents the EVM of the re-transmitted signal without implementing the Pre-Equalization stage, from which it can be observed that it presented the worst EVM. On the other hand, from Figure 12, it can be noted that, when the Pre-Equalization stage was implemented in the A&F Relay Node, the error gradually decreased. Furthermore, it was found that, when the A&F-ZF RN was employed, the EVM was higher than when the A&F-MMSE RN was used. Besides, the authors have verified that the power of the re-transmitted RG from the A&F protocol was degraded on an order of 17.7 dB in comparison to the transmitted RG from the eNB.

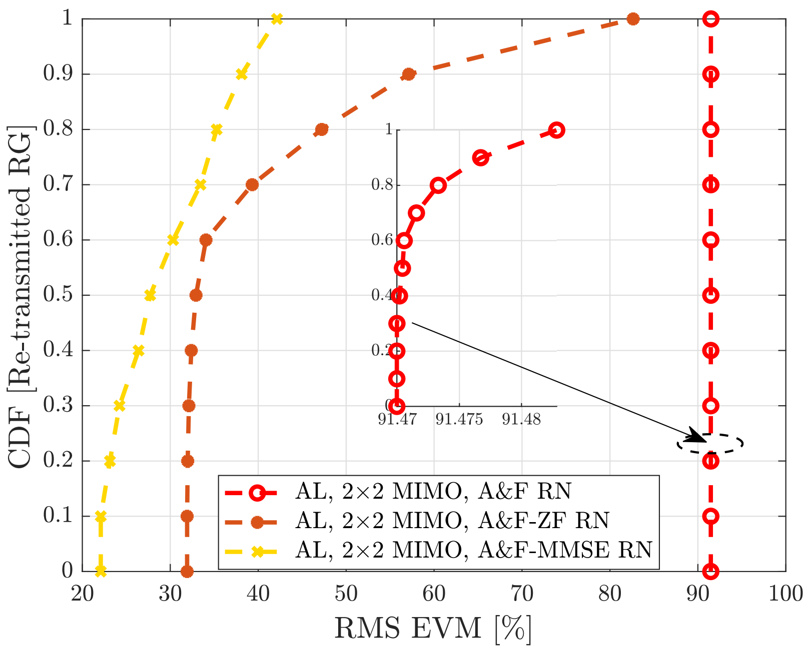

Figure 12. EVM of the Re-transmitted Resource Grid from A&F Relay Node.

6.2. Performance Evaluation of MIMO RNCS

Figure 13 shows the BER performance as a function of SNR for a MIMO A&F RN with or without pre-qualification techniques and for a D&F RN for two different transmission schemes (SISO and MIMO). Another plot corresponding to the performance of a 2 × 2 MIMO link between the eNB and the UE has been included in the graph. We note that, in the figure, DL represents the received signal of the UE through the direct link, while AL symbolizes the signal received at the UE by means of the access link. From the achievable BER performance shown in Figure 13, it can be seen that the RNCS significantly increased the system performance, in comparison with the Non-Co-operative System with 2 × 2

MIMO scheme. Furthermore, we note that the A&F with pre-equalization techniques obtained better BER performance than the conventional 2 × 2 MIMO A&F strategy. In this context, it can be seen that the A&F-ZF pre-equalization system achieved a BER level of 1.39×10^{-2} at around SNR = 14 dB while, with A&F-MMSE pre-equalization, the RNCS reached the same BER level at around SNR = 11 dB, such that a performance gain of 3 dB was achieved. Therefore, the MMSE pre-equalization scheme is capable of improving the system performance, which was achieved as this scheme considered the noise in its process of equalization.

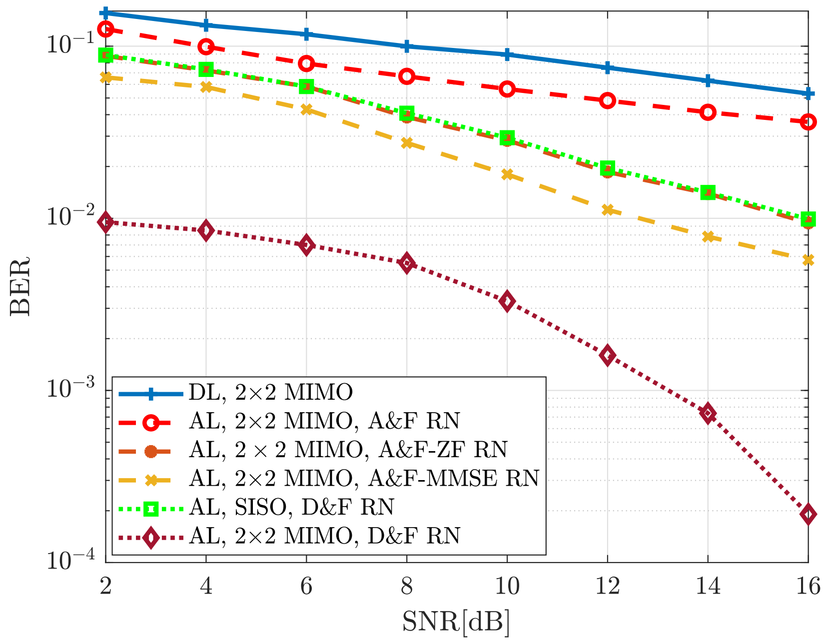

Figure 13. BER performance of the implemented RNCS, in comparison with a conventional MIMO system.

On the other hand, when we used the SISO D&F strategy, the system reached approximately the same BER level as the A&F-ZF protocol, at around SNR = 10 dB, implying that 6 dB performance gain was successfully achieved, compared to the performance of the conventional MIMO A&F protocol without pre-equalization scheme. This is due to the improvements that the decoding and encoding processes carried out by the D&F Relay Nodes introduce into the re-transmitted signal, which in this case are sufficient to compensate for the improvements due to the MIMO capacity and the Zero-Forcing pre-equalization technique of the A&F Relay Node. It can be seen, from Figure 13, that the 2 × 2 MIMO D&F protocol generally achieved better BER performance than both the 2 × 2 MIMO Non-Co-operative System and the 2 × 2 MIMO A&F conventional with or without pre-equalization schemes. More specifically, the 2 × 2 MIMO D&F protocol achieved the same performance as the 2 × 2 MIMO A&F-MMSE at SNR = 8 dB, such that an 8 dB performance gain was attained. Finally, the 2 × 2 MIMO D&F co-operative system obtained the better BER performance between the considered co-operative techniques, which is achieved by means of the decoding and encoding steps that the received signal is subjected before being re-transmitted to the UE through the $\mathbf{H}^2$ channel.

The achievable capacity performance recorded for the 2 × 2 MIMO Non-Co-operative System and 2 × 2 MIMO RNCS, the latter with various Relay Node schemes, is shown in Figure 14. It can be observed, from the figure, that the MIMO Co-operative System achieved higher average throughput than the MIMO Non-Co-operative System. It may also be seen that, when the pre-equalization techniques were introduced before re-transmitting the signal in the A&F protocol, the achievable throughput of the RNCS increased. Figure 14 indicates that the throughput of the 2 × 2 MIMO A&F-ZF Co-operative System at SNR = 12 dB was approximately 10.35 Mbps while, with the 2 × 2 MIMO A&F-MMSE protocol, a throughput of 11.37 Mbps could be reached with the same SNR value, such that a performance gain of about 1.02 Mbps was achieved. Moreover, with the SISO D&F protocol, a maximum capacity of 11.20 Mbps was obtained, associated with a performance gain of 5.92 Mbps, in comparison with MIMO Non-Co-operative System.

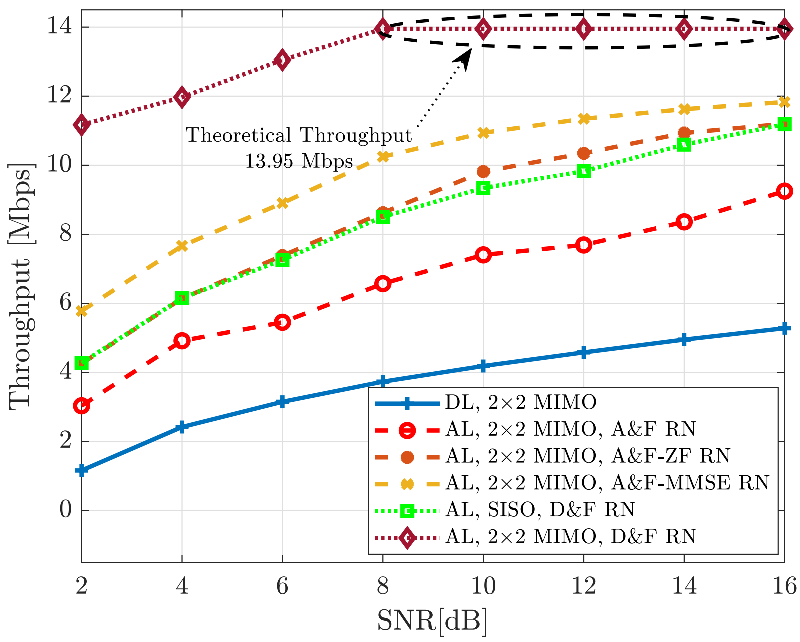

Figure 14. Achievable throughput comparison of the implemented RNCS with a conventional MIMO system.

On the other hand, when compared with the MIMO A&F conventional strategy with or without pre-equalization scheme, the SISO D&F protocol achieved better capacity than the MIMO A&F conventional without pre-equalization, as can be seen in Figure 14; moreover, considering the pre-equalization schemes, the SISO D&F protocol reached approximately the same capacity as the A&F-ZF strategy. We also present the throughput of the 2 × 2 MIMO D&F Co-operative System, which substantially improved the system throughput. More explicitly, the theoretical capacity of 64-QAM (13.95 Mbps is the total possible capacity per frame that our system would obtain when using the 64-QAM constellation and without any channel. This theoretical capacity has been calculated considering an ideal simulation (without channel and noise).) was reached at SNR =8 dB. Furthermore, the obtained throughput minimum was 11.17 Mbps, which could be achieved with the 2 × 2 MIMO A&F-MMSE strategy at SNR =14 dB.

6.3. Complexity and Comparative Discussion

In this subsection, we analyze the complexity of the relaying protocols, in terms of hardware and arithmetic operations. From the hardware implementation, all Relay Nodes are developed with the same components (one NI-USRP 2944R and PC), which were described above. Nevertheless, from the point of the number of operations required to carry them out, as a function of the dimensions of the vectors and matrices involved present significant differences.

In this sense, it can be shown in Table 2, which summarizes the arithmetic operations that the proposed protocols require to capture and forward the received signal to the UE. From Table 2 can be noticed that the strategy with less complexity is the A&F Relay Node, which $\mathrm{N_T^R N_R^R T}$ and $\mathrm{N_T^R T(N_R^R - 1)}$, products and summations, respectively, are required. However, the A&F protocol with the pre-equalization stage increases your computational complexity in comparison with A&F conventional strategy. In this regard, both strategies, A&F-ZF and A&F-MMSE perform one first step of channel estimation, and after that a stage of equalization. In this sense, the A&F-MMSE presents major complexity than A&F-ZF relaying.

On the other hand, the D&F scheme is the more complex between the implemented strategies, as can be observed in Table 2, due to the decoding and encoding processes, which are performed to the received signal. It should be noticed that $N_T^R \times N_R^R$ is the combiner antennas in the protocols and $\lambda \times \alpha = P$ describes the total number of the pilot symbols. Besides, μ exemplifies the total number of the data symbols, which are employed to implement the Bi-Cubic Interpolate. From this subsection, it can be seen that the computational complexity of the D&F Relay Node was higher than the rest of the developed protocols.

Table 2. Arithmetic operations required by Relay Node Protocols.

RN Protocols	Products	Summations	Flops
A&F	$N_T^R N_R^R T$	$N_T^R T(N_R^R - 1)$	$2N_T^R N_R^R T - N_T^R T$
A&F-ZF	$N_T^S N_R^R[\frac{\lambda\alpha(\alpha+1)}{2} + 20\mu + \frac{7T^3+3T^2-4T}{6}] + N_T^R N_R^R T$	$N_T^S N_R^R[\frac{\alpha(\lambda-1)(\alpha+1)}{2} + 74\mu + \frac{7T^3+9T^2+2T}{6}] + N_T^R T(N_R^R - 1)$	$N_T^S N_R^R[\frac{\alpha(\alpha+1)}{2}(2\lambda - 1) + 94\mu + \frac{7T^3+6T^2-T}{3}] + 2N_T^R N_R^R T - N_T^R T$
A&F-MMSE	$N_T^S N_R^R[\frac{\lambda\alpha(\alpha+1)}{2} + 20\mu + \frac{7T^3+9T^2-4T}{6}] + N_T^R N_R^R T$	$N_T^S N_R^R[\frac{\alpha(\lambda-1)(\alpha+1)}{2} + 74\mu + \frac{7T^3+15T^2+2T}{6}] + N_T^R T(N_R^R - 1)$	$N_T^S N_R^R[\frac{\alpha(\alpha+1)}{2}(2\lambda - 1) + 94\mu + \frac{7T^3+12T^2-T}{3}] + 2N_T^R N_R^R T - N_T^R T$
D&F	$N_T^S N_R^R[\frac{\lambda\alpha(\alpha+1)}{2} + 20\mu + \frac{7T^3+9T^2-4T}{6}] + T[N_s N_R^R + N_T^R(N_s + N_R^R)]$	$N_T^S N_R^R[\frac{\alpha(\lambda-1)(\alpha+1)}{2} + 74\mu + \frac{7T^3+15T^2+2T}{6}] + T[N_s(N_R^R - 1) + N_T^R(N_s + N_R^R - 2)]$	$N_T^S N_R^R[\frac{\alpha(\alpha+1)}{2}(2\lambda - 1) + 94\mu + \frac{7T^3+12T^2-T}{3}] + T[N_s(2N_R^R + 2N_T^R - 1) + N_R^R(N_R^T + 1) - 2N_T^R]$

The proposed RNCS is compared with prior works, in terms of the type of implemented strategy and developed hardware, as shown in Table 3. In general, in [11,16,38] works and proposed architecture, the performance of the A&F and D&F strategies have been analyzed and compared, showing that the usage of a co-operative system improves the network capacity and the D&F protocol presents higher behavior than the A&F Relay Node architecture.

Table 3. A comparison survey with previous works.

Parameters	[11]	[16]	[38]	Proposed
Signal Model	Conventional	Conventional	Conventional	LTE
A&F RN	Yes	Yes	No	Yes
A&F-ZF RN	No	No	No	Yes
A&F-MMSE RN	No	No	No	Yes
D&F RN	No	Yes	Yes	Yes
Flexibility	Yes	Yes	Yes	Yes
Hardware	USRP	FPGA	USRP	USRP
Software	Labview	-	GNU	Matlab
Modulation Scheme	8-PSK	Q-PSK	G-MSK	64-QAM
Protocol Comparison	No	Yes	No	Yes

The main limitation found in the related works is the considered signal. In this sense, in the analyzed studies, signal models don't fulfil the requirement of the standardized by the 3GPP [13], as have been in this paper (LTE). Besides, in this paper have also proposed several hardware implementation of the relaying protocols, which in the literature, a deep comparative study has not been taken into account.

7. Conclusions

In this paper, a detailed study and implementation of a Relay Node Co-operative System based on a Software Defined Radio (SDR) Platform and the Matlab^{TM} tool has been performed in order to enhance the average system throughput and BER in indoor-to-indoor environments. The architecture implements a Relay Node Cooperative Network, which uses in-band Relaying Protocols. Two protocols of Relay Nodes have been developed: Amplify-&-Forward (A&F) and Decode-&-Forward (D&F). Moreover, Pre-Equalization stages for the A&F relay were studied, considering the Zero Forcing and Minimum Mean Square Error Pre-Equalization schemes. The cooperative system deploys Relay Node with one antenna at transmission and one antenna at reception, as well as, multiple antennas. Furthermore, the 4G signal employs features that are standardized by the 3GPP. Our measurement results demonstrated the viability and flexibility of the Co-operative System developed through the SDR and Matlab^{TM} software.

On the other hand, the results demonstrated that the Co-operative System clearly outperforms the Non-Co-operative architecture. Furthermore, it can be seen that the A&F protocol with the pre-equalization technique greatly enhances the Key Performance Indicators of the system in comparison with the A&F conventional strategy. For example, the maximum throughput of the A&F protocol with Pre-equalization stage is 11.83 Mbps at SNR = 16 dB. However, with A&F conventional strategy, the reached result is less, which has obtained losses of approximately 1.94 Mbps of the maximum throughput achieved by the A&F-ZF protocol at SNR = 16 dB. From the results, it is concluded that the A&F-MMSE strategy presents higher performance than the A&F-ZF scheme, due to the less EVM of the re-transmitted Resource Grid to the UE in the second stage. It can be noticed that the SISO D&F Co-operative Network presents approximately the same performance that 2×2 MIMO A&F-ZF protocol. Nevertheless, the implemented MIMO D&F Relay Node showed the best performance of the different strategies implemented. In this context, the maximum throughput of the proposed Two-Hop Co-operative System for 64-QAM signal (13.95 Mbps) is reached from SNR = 8 dB, when the MIMO D&F Relay Node is used, being the only one strategy that can achieve it. Furthermore, it can be concluded from the results that employing Relay Node together MIMO technique led to a substantial benefit, in terms of the KPIs of the network in the indoor-to-indoor environment. The MIMO scheme achieved a reduction of the Bit Error Rate (BER) and increasing the throughput in the 64-QAM modulation scheme, which can be concluded increasing the number of antennas can lead to higher performance and spectral efficiency of the system. In addition, the D&F algorithm is the most complex between the developed protocols, due to the decoding and encoding processes. We believe that the implemented platform provides a cost-effective, scalable, and easy to update solution for enabling 5G signals standardized by the 3GPP.

Author Contributions: R.V.-P. conceived the paper, designed the experiments, performed experiments, analyzed the data and wrote the paper; R.V.-P. and J.I.A. reviewed and edited the paper. All authors have read and agreed to the published version of the manuscript.

Funding: This work has been supported by the Spanish Ministry of Science, Innovation and Universities within the project TEC2017-87061-C3-1-R (CIENCIA/AEI/FEDER,UE) and by the China Science and Technology Exchange Center-MST of the People's Republic of China, within the project 23016YFE0200200. The work of Randy Verdecia-Peña is supported by a Pre-doctoral Contract PRE2018-085032 from the Ministry of Science and Innovation.

Conflicts of Interest: The authors declare no conflict of interest.

References

1. Yahya, A. *LTE-A Cellular Networks. Multi-hop Relay for Coverage, Capacity and Performance Enhancement*; Springer: Cham, Switzerland, 2017.
2. Krikidis, I.; Zheng, G. *Advanced Relay Technologies in Next Generation Wireless Communications*; The Institution of Engineering and Technology: London, UK, 2016.
3. Fan, Y.; Thompson, J. MIMO Configurations for Relay Channels: Theory and Practice. *IEEE Trans. Wirel. Commun.* **2007**, *6*, 1774–1786. [CrossRef]
4. He, Z.; Yang, J.; Wang, X.; Liu, Y.; Rong, Y. Channel Estimation of MIMO Relay Systems With Multiple Relay Nodes. *IEEE Access* **2017**, *5*, 27649–27658. [CrossRef]
5. Marina, N.; Kavcic, A.; Gaarder, N.T. Capacity Theorems for Relay Channels with ISI. In Proceedings of the 2008 IEEE International Symposium on Information Theory, Toronto, ON, Canada, 6–11 July 2008. [CrossRef]
6. Laneman, J.N.; Tse, D.N.C.; Wornell, G.W. Cooperative Diversity in Wireless Networks: Efficient Protocols and Outage Behavior. *IEEE Trans. Inform. Theor.* **2004**, *50*, 3062–3080. [CrossRef]
7. Kramer, G.; Gastpar, M.; Gupta, P. Cooperative Strategies and Capacity Theorems for Relay, Networks. *IEEE Trans. Inform. Theor.* **2005**, *51*, 3037–3063. [CrossRef]
8. Cao, Y.; Chen, B. Capacity bounds for two-hop interference networks. In Proceedings of the 2009 47th Annual Allerton Conference on Communication, Control, and Computing (Allerton), Monticello, IL, USA, 30 September–2 October 2009.
9. Torabi, M.A.; Frigon, J.F. A decomposition approach to MIMO interference relay networks. In Proceedings of the IEEE GLOBECOM 2008—2008 IEEE Global Telecommunications Conference, New Orleans, LA, USA, 30 November–4 December 2008.
10. Truong, K.T.; Sartori, P.; Heath, R.W. Cooperative Algorithms for MIMO Amplify-and-Forward Relay Networks. *IEEE Trans. Signal Process.* **2013**, *61*, 1272–1287. [CrossRef]
11. Tanoli, S.A.K.; Rehman, M.; Khan, M.B.; Jadoon, I.; Ali Khan, F.; Nawaz, F.; Shah, S.A.; Yang, X.; Nasir, A.A. An Experimental Channel Capacity Analysis of Cooperative Networks Using Universal Software Radio Peripheral (USRP). *Sustainability* **2018**, *10*, 1983. [CrossRef]
12. Rani, R.; Singh, S. Performance Analysis of SDR based Wireless Relay Networks. In Proceedings of the 2018 10th International Conference on Computational Intelligence and Communication Networks (CICN), Esbjerg, Denmark, 17–19 August 2018.
13. 3GPP. Evolved Universal Terrestrial Radio Access (E-UTRA). User Equipment (UE) Radio Transmission and Reception. ETSI TS 36.101. 2017; Volume 36, p. 14. Available online: https://www.etsi.org/deliver/etsi_ts/136100_136199/136101/14.03.00_60/ts_136101v140300p.pdf (accessed on 30 January 2021).
14. 3GPP. Evolved Universal Terrestrial Radio Access (E-UTRA). Relay Architectures for E-UTRA (LTE-Advanced). ETSI TS 36.806. 2010; Volume 36, p. 9. Available online: ftp://ftp.freecalypso.org/GSM/3GPP/archive/36_series/36.806/36806-900.pdf (accessed on 30 January 2021).
15. 3GPP. Evolved Universal Terrestrial Radio Access (E-UTRA); Further Advancements for E-UTRA Physical Layer Aspects. ETSI TS 36.814. 2017; Volume 36, p. 9. Available online: https://pdfs.semanticscholar.org/d6e8/93efee6bcd1654321eec6a44130fa5b016fe.pdf (accessed on 30 January 2021).
16. Zetterberg, P.; Mavrokefalidis, C.; Lalos, A.S.L.; Matigakis, E. Experimental Investigation of Cooperative Schemes on a Real-Time DSP-Based Testbed. *J. Wirel. Commun. Netw.* **2009**, 368752. [CrossRef]
17. Wireless Open Access Research Platform. Available online: http://warp.rice.edu/index (accessed on 20 April 2020).
18. Marín-García, J.A.; Romero-Franco, C.; Alonso, J.I. A Software Defined Radio Platform for Decode and Forward Relay Nodes Implementation. In Proceedings of the 2019 IEEE Conference on Standards for Communications and Networking (CSCN), Málaga, Spain, 28–30 October 2019.
19. Verdecia-Peña, R.; Alonso, J.I. An enhanced Software Defined Radio Platform for evaluation of Decode&Forward Relay Nodes. In Proceedings of the XXXV Simposio Nacional de la Unión Científica Internacional de Radio, URSI 2020 (URSI20), Málaga, Spain, 2–4 September 2020.
20. Berger, S.; Kuhn, M.; Wittneben, A.; Unger, T.; Klein, A. Recent advances in amplify-and-forward two-hop relaying. *IEEE Commun. Mag.* **2009**, *47*, 50–56. [CrossRef]
21. Ikki, S.S.; Ahmed, M.H. Performance analysis of adaptive decode-and-forward cooperative diversity networks with best-relay selection. *IEEE Trans. Commun.* **2010**, *58*, 68–72. [CrossRef]
22. Oliva Sánchez, J.D.; Alonso, J.I. A Two-Hop MIMO Relay Architecture Using LTE and Millimeter Wave Bands in High-Speed Trains. *IEEE Trans. Veh. Technol.* **2019**, *68*, 2052–2065. [CrossRef]
23. Sanz-Gómara, A.; Marín-García, J.A.; Alonso, J.I. A Performance Evaluation of MIMO Architectures with Moving Relays in High-Speed Railways. In Proceedings of the IEEE 48th European Microwave Conf. (EuMC), Madrid, Spain, 23–27 September 2018.
24. Rong, Y. Linear non-regenerative multicarrier MIMO relay communications based on MMSE criterion. *IEEE Trans. Commun.* **2010**, *58*, 1918–1923. [CrossRef]
25. Toding, A.; Khandaker, M.R.A.; Rong, Y. Joint source and relay optimization for parallel MIMO relay networks. *EURASIP J. Adv. Signal Process.* **2012**, *174*. [CrossRef]
26. Rong, Y.; Hua, Y. Optimality of diagonalization of multi-hop MIMO relays. *IEEE Trans. Wirel. Commun.* **2009**, *8*, 6068–6077. [CrossRef]

27. Lioliou, P.; Viberg, M.; Coldrey, M. Efficient channel estimation techniques for amplify and forward relaying systems. *IEEE Trans. Commun.* **2012**, *60*, 3150–3155. [CrossRef]
28. Rong, Y.; Khandaker, M.R.A.; Xiang, Y. Channel estimation of dual-hop MIMO relay system via parallel factor analysis. *IEEE Trans. Commun.* **2012**, *11*, 2224–2233. [CrossRef]
29. Chiong, C.W.R.; Rong, Y.; Xiang, Y. Channel estimation for two-way MIMO relay systems in frequency-selective fading environments. *IEEE Trans. Commun.* **2015**, *14*, 399–409. [CrossRef]
30. Chiong, C.W.R.; Rong, Y.; Xiang, Y. Channel estimation for time-varying MIMO relay systems. *IEEE Trans. Wirel. Commun.* **2015**, *14*, 6752–6762. [CrossRef]
31. Wang, J.; Wang, G.; Zheng, L.; Wang, H. Two-Way Amplify-Forward MIMO Relay Systems Using MMSE Pre-Equalization. In Proceedings of the 10th International Conference on Communications and Networking in China (China Com), Shanghai, China, 15–17 August 2015.
32. Hsieh, M.H.; Wei, C.H. Channel estimation for OFDM systems based on comb-type pilot arrangement in frequency selective fading channels. *IEEE Trans. Consum. Electron.* **1998**, *44*, 217–225. [CrossRef]
33. Acar, Y.; Doğan, H.; Başar, E.; Panayirci, E. Pilot Symbol Aided Channel Estimation for Spatial Modulation-OFDM Systems and its Performance Analysis with Different Types of Interpolations. *Wirel. Pers. Commun.* **2017**, *94*, 1387–1404. [CrossRef]
34. Endo, C.; Miyazaki, H.; Adachi, F. Space-time block coded amplify-and-forward cooperative relay without channel state information at relay station. In Proceedings of the 2014 International Symposium on Wireless Personal Multimedia Communications (WPMC), Sydney, Australia, 7–10 September 2014.
35. Han, Y.; Meng, W.; Zhang, Y. Adaptive decode-and-forward cooperative diversity with multiple-antenna terminals. In Proceedings of the 2011 6th International ICST Conference on Communications and Networking in China (CHINACOM), Harbin, China, 17–19 August 2011.
36. Kumar, D.P.; Babu, M.S.; Prasad, M.S.G. Suboptimal comparison of AF and DF relaying for fixed target error probability. In proceedings of the 2016 International Conference on Computer Communication and Informatics (ICCCI), Coimbatore, India, 7–9 January 2016.
37. Building a Cooperative Communications System. Available online: http://warp.rice.edu/ (accessed on 20 April 2020).
38. Prince, A.; Abdalla, A.E.; Dahshan, H.; Rohiem, A.E.D. Performance evaluation of multihop decode and forward cooperative relaying. In Proceedings of the 2017 International Conference on Advanced Control Circuits Systems (ACCS) Systems & 2017 International Conference on New Paradigms in Electronics & Information Technology (PEIT), Alexandria, Egypt, 5–8 November 2017.
39. Verdecia-Peña, R.; Alonso, J.I. MIMO Channel Estimation in an SDR Platform for Evaluation of D&F Relay Nodes. *Electronics* **2020**, *10*, 1662. [CrossRef]
40. Wang, M.; Zhang, J.; Ren, B.; Yang, W.; Zou, J.; Hua, M.; You, X. The Evolution of LTE Physical Layer Control Channels. *IEEE Commun. Surv. Tutor.* **2016**, *18*, 1336–1354. [CrossRef]
41. Sanchez, J.J.; Morales-Jimenez, D.; Gomez, G.; Enbrambasaguas, J.T. Physical Layer Performance of Long Term Evolution Cellular Technology. In Proceedings of the 2007 16th IST Mobile and Wireless Communications Summit (ISTMWC), Budapest, Hungary, 1–5 July 2007; pp. 1–5. [CrossRef]
42. Van de Beek, J.J.; Edfors, O.; Sandell, M.; Wilson, S.K.; Borjesson, P.O. On Channel Estimation in OFDM Systems. In Proceedings of the IEEE 45th Vehicular Technology Conference Countdown to the Wireless Twenty-First Century, Chicago, IL, USA, 25–28 July 1995.
43. Wang, H.F.; Chen, M.S.; Lin, C.H.; Hwang, C.P. *Channel Equalization for MIMO LTE System in Multi-Path Fading Channels*; Springer: Singapore, 2016.
44. 3GPP. LTE; Evolved Universal Terrestrial Radio Access (E-UTRA). Base Station (BS) Radio Transmission and Reception. ETSI TS 36.104. 2017; Volume 36, p. 14. Available online: https://www.etsi.org/deliver/etsi_ts/136100_136199/136104/14.03.00_60/ts_136104v140300p.pdf (accessed on 30 January 2021).